Wesleyan University

Measurements of Effective Temperature Variations in the Host Star of a Transiting Exoplanet

by

Erin Arai

A thesis submitted to the
faculty of Wesleyan University
in partial fulfillment of the requirements for the
Degree of Masters of Arts
in Astronomy

Middletown, Connecticut April, 2010

The story so far: In the beginning the Universe was created. This has made a lot of people very angry and has been widely regarded as a bad move.

–Douglas Adams

The Restaurant at the End of the Universe

Contents

Chapter 1

Introduction

The term 'planet' has held a variety of meanings throughout the course of history. Its precise definition was revised in 2005 after the discovery of trans-Neptunian body Eris, an object larger than Pluto, previously accepted as our solar system's smallest planet. As of 2006 the International Astronomy Union (IAU) has defined a planet as "a celestial body that (a) is in orbit around the Sun, (b) has sufficient mass for its self-gravity to overcome rigid body forces so that is assumes a hydrostatic equilibrium (nearly round) shape and (c) has cleared the neighborhood around its orbit."

The first exoplanet was discovered in 1992 around pulsar PSR-1252+12 by Aleksander Wolszczan and Dale Frail (Wolszczan & Frail 1992). This marked the advent of a new sub-field of astronomy, whose development has been facilitated in recent years by huge technological advances. There are now 446 exoplanets known (exoplanet.eu 2010), and the number increases daily. In the past decade there have been numerous exoplanet detection surveys, including but not limited to CoRot, HAT, Kepler, OGLE, TrES, XO, and HAT. The growing number of discovered exoplanets has led to an enormous amount of follow-up and auxiliary observations, the analyses of which has spurred research ranging from exoplanetary composition to planetary migration and formation.

To further improve our understanding of planetary systems, we must under-

stand stellar behavior and its impact on planets. Many exoplanetary systems are complicated by the stellar variability of the host star; main sequence solar-mass dwarfs are often highly variable (Hall et al. 2007). In our own solar system, the Sun's variability (which has a period of about 11 years) has had significant effects on Earth. During periods of high stellar activity, the Sun is home to star spots, which are the visible manifestation of localized magnetic fields. A recent cool period, the Little Ice Age, is thought to have coincided with a period of very low solar activity, the Maunder Minimum (Luterbacher et al. 2004).

1.1 Exoplanet Detection

Exoplanets can be detected in several ways, but the two most common are the transit method and the radial velocity method. To date approximately 15% of exoplanet detections have been made via the transit method, and the other 85% using the radial velocity method. There are several other methods that have been used (microlensing, pulsar timing, etc.) but they make up a very small fraction of the total number of detections. The transit method involves monitoring luminosity of the host star for periodic dimmings, which correspond to the planet passing in front of the star see Figures 1.1 and 1.2. This method has several limitations and biases. Firstly, the number of systems that are oriented such that we can observe a transit is limited (though random). The method is also better suited to detecting large, close-in planets. The larger the planet, the more pronounced the aforementioned eclipse because the projection of the planet onto the star is larger. Small planetary orbital radii also favor this technique because the closer a planet is to its star, the more frequently it transits and the larger the range of inclination angles that still result in a transit.

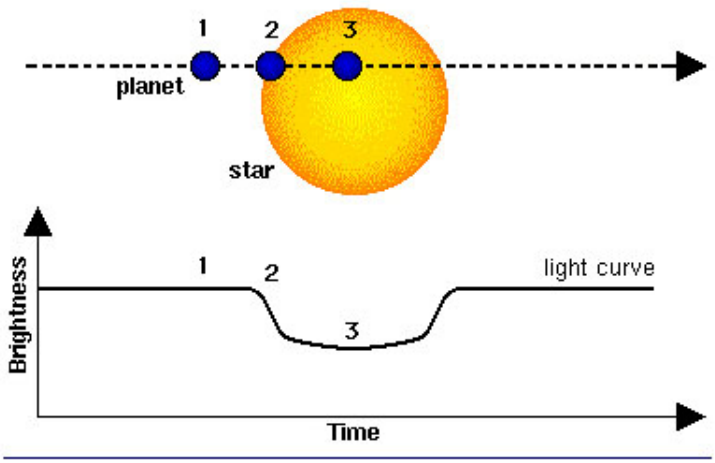

Figure 1.1: A schematic of an exoplanet transit (CNES, 2010).

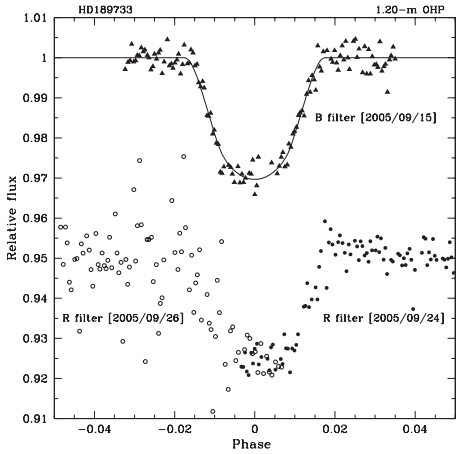

Figure 1.2: HD189733's transit light curve as observed by Bouchy et al. (2005).

The radial velocity method is similarly biased towards detecting close, large planets, although it does not require the system of interest to have as specific an orientation with respect to us as the transit method. The radial velocity method of planet detection relies on monitoring variations in the host stars periodic Doppler shift as the star orbits the center of mass of the system, which is offset from the center of the star due to the presence of another massive object (in our case, a planet)(Figure 1.1). This is done by the displacement of the host stars spectral

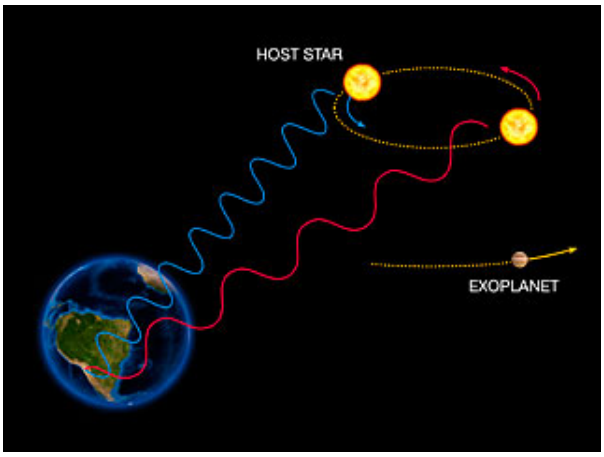

Figure 1.3: A schematic of a stellar wobble as induced by an exoplanet. It is this effect that the radial velocity method takes advantage of (ESO, 2010)

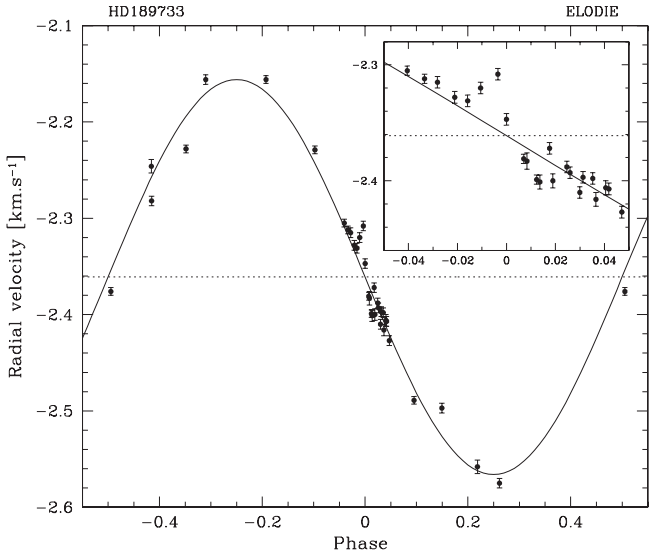

Figure 1.4: HD189733's radial velocity light curve as observed by Bouchy et al. (2005).

lines. This method works for a far wider range of inclination angles, although if the system is completely face-on it is ineffective. HD189733's radial velocity curve is shown in Figure 1.4.

Table 1.1: HD189733 System Parameters

Stellar Radius	$0.781 \pm 0.051 R_{\odot}$	(van Belle & von Braun 2009)
Stellar Mass	$0.82 \pm 0.03 M_{\odot}$	(Bakos et al. 2006)
Stellar Rotation Period	11.953± .009 days	(Henry & Winn 2008)
Planet Orbital Period	2.2185733± .00002 days	(Bouchy et al. 2005)
Effective Temperature	4939± 158 K	(van Belle & von Braun 2009)
Planet Mass	$1.15 \pm 0.04 M_{Jupiter}$	(Bouchy et al. 2005)
Planet Radius	$1.26 \pm 0.03 R_{Jupiter}$	(Bouchy et al. 2005)
Spectral Type	K1.5V/M	(Bouchy et al. 2005)

1.2 HD189733

HD189733 (also catalogued as V452 Vulpeculae) is a binary star system consisting of a K1.5 dwarf star and a red dwarf star. It is located about 19.5 parsecs away in the constellation of Vulpecula. The primary star (the K1.5 dwarf) is variable and as a result also has a variable star designation V452 Vul.

The exoplanet HD189733b was confirmed in 2005 (Bouchy et al. 2005). It is approximately 1.13 Jupiter-masses and orbits the primary star with a period of $\sim$ 2.2 days (Bouchy et al. 2005), see Table 1.1. HD189733 is one of the most studied exoplanetary systems because it is relatively close and bright ($m_v \sim 7.676$). As previously mentioned, HD189733 is known to be photometrically variable on different time scales (Henry & Winn 2008). Henry & Winn (2008) found the stellar rotation period to be 11.953 ± .009 days using synoptic optical photometry (**??**). They monitored HD189733 from October 2005 to July 2007 and used the observed photometric variability to derive a stellar rotation period. HD189733 is a moderately difficult source to obtain a rotation period for because it is so highly active that stellar activity features (like spots) change frequently. Thus the

rotation period calculated from their data may coincide exactly with the rotation period derived from observations taken over a different period of time.

1.3 Stellar Atmospheres

Stellar atmospheres are the primary observables for the rest of stellar physics. A solid understanding and interpretation of data and what they imply about the inner workings of stars is paramount if we are to fully appreciate the physical means by which stars radiate! The behavior of a stellar atmosphere is dictated by its density and emergent energy, which correspondingly depend on the mass, age, and chemical composition of the star. Stellar atmospheres can be broadly broken down into four sections, the sub-photosphere, the photosphere, the chromosphere and the corona. Most visible light that we observe comes from the photosphere, which is governed largely by two fundamental parameters, the star's surface gravity and temperature. The width, or height of the photospheric layer is inversely proportional to the star's surface gravity. Photospheres are not generally one temperature - there may be up to a factor of two between the temperature at the top of the layer and the temperature at the bottom of the layer. It is standard to describe the photospheric temperature by the star's effective temperature, which is defined as the total power per unit area radiated by the star:

$$L = 4\pi R^2 \int_0^\infty F_\nu d\nu = 4\pi R^2 \sigma T_{eff}^4$$

A star (and therefore its photosphere) is often holistically described by its spectral type, which is determined by the relative strengths and shapes of photospheric absorption lines. Essentially, photospheres act like cool envelopes around hot interiors, which results in an absorption line spectrum that we can observe

(with a spectrograph). Spectral types on a typical HR-diagram span from O stars, the hottest and most luminous, to M stars, the faintest and coolest. There are ten subdivisions per letter (O, B, A, F, G, K, M), and there is also an extension of the system for brown dwarfs (L, T).

1.4 Stellar Variability

Stellar variability can manifest itself in various ways. In some cases variability is regular and its period and amplitude can be precisely established. Mechanisms behind stellar variability range from a pulsating balance between pressure, temperature and opacity to active stellar dynamos. Effects can take the form of flares and/or star spots that are related to the star's magnetic activity.

Being able to accurately model stellar variability is especially important when considering possible planet-star interactions. In the case of HD189733 we have to carefully consider variations due solely to stellar phenomenon (flares, spots etc.) and variations that may be caused by interaction with the planet (also flares, spots, tidal bulging). We use high resolution spectra (R $\sim$ 60,000) to monitor the ratios of many photospheric absorption lines to look for variation on several timescales including the rotation period of the star and the orbital period of the planet.

1.5 Importance of our work

Our analysis involves using the line depth ratio (LDR) technique (which will be elaborated upon Chapter 2) to make precise effective temperature measurements, which we ultimately correlate with time. Temporal temperature variations can be indicative of a variety of phenomenon, including stellar variability due to planet

star interactions (PSIs).

There have been several studies done in the past 10 years that have utilized line depth ratios to study both giant and dwarf stars. The past few years have seen several efforts to detect, monitor and quantify PSIs (Fares et al. 2010). What we bring to the table is the combination: using LDRs to (hopefully) characterize PSIs. There are only a few other groups that have used a large number of co-added line depth ratios (on the order of hundreds) to analyze stellar temperature variations (Kovtyukh et al. 2003). Relative effective temperature variations may well be symptoms of PSIs, and the LDR method is one of the best ways to quantify temporal temperature changes (if you have high resolution spectroscopy of your object of course!). Thus we hope our work will help to refine the LDR method, while at the same time potentially shedding new light on PSIs.

Besides studying PSIs, which may have exciting implications for planetary migration and close-in planet survival, the method of LDRs is useful unto itself to understand the temperature structure of stars and is worthy of use, study, and refinement. The efficacy of LDRs as robust indicators of effective temperature was assessed (to be good) by Gray & Livingston (1997). Biazzo et al. (2004) devised an LDR technique that used medium resolution ($R = \frac{\lambda}{\Delta\lambda}$) spectroscopy to measure the modulation of average surface temperature to within 10 K in spotted active stars and Cepheid pulsating variables (Biazzo et al. 2004).

The general progression of this document is as follows: the next chapter provides the background necessary to understand why LDRs work and why they are worth bothering with. This essentially just requires some understanding of stellar photospheres and their dependence on certain physical parameters. Then we briefly discuss our data, how they were obtained and the instrument they were observed with. The next section describes our analysis, which was really the pri-

mary part of this thesis. We then discuss our results, make a few conclusions, and offer ideas regarding how we will continue to approach this project (as it is not yet finished) and what other areas of future research may also be able to utilize LDRs.

Chapter 2

Background

2.1 Line Depth Ratio Basics

At this point it is instructive to have a basic understanding of the LDR method and what it requires, in order to motivate the next part of the discussion. The LDR method firstly requires a well-fit stellar continuum and well-fit absorption or emission lines, making high resolution spectroscopy a necessity. (I shall proceed assuming that we are dealing with absorption lines, but the method can be executed using either sort of line. Of course, if one is using emission lines, one is generally not dealing with radiation in the visible part of the electromagnetic spectrum or from the stellar photosphere. Emission lines usually originate where the continuum is relatively low, like in the transition region between the chromosphere and the corona, and are visible in the UV).

Different transitions (and thus different absorption lines) have different temperature dependences (see Figure 2.1). In general, for LDRs, results are only accurate if non-saturated, metallicity-independent lines are used (usually weak metal lines, this will be discussed in section 2.3). For now, suffice it to say, the best ratios to choose are those whose lines have opposite temperature dependences, but are not dependent on other stellar parameters (like metallicity). It is worthwhile to note that while LDRs are extremely useful for precisely mea-

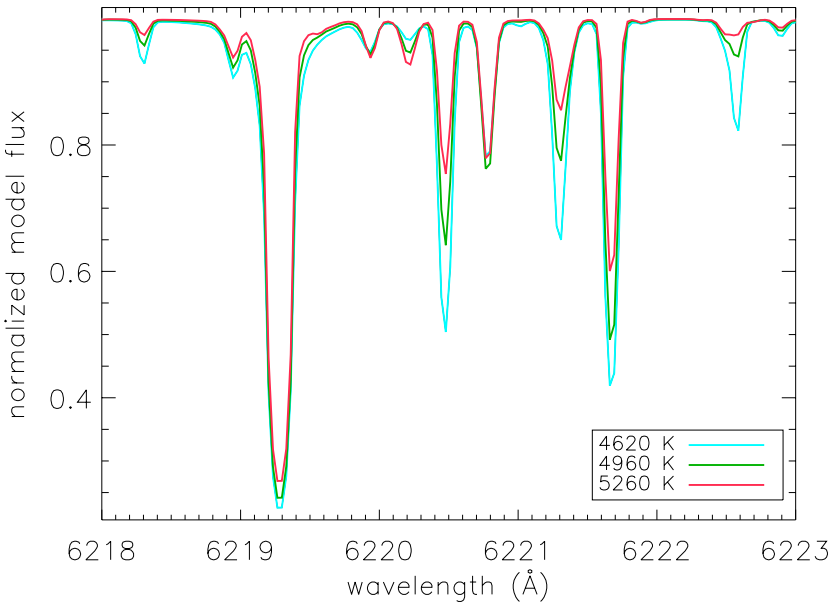

Figure 2.1: Example of the temperature dependence of weak metal photospheric lines.

suring relative temperature change, they are not useful for measuring absolute temperatures because absolute temperature calibration is itself not very precise. It would be silly to try to measure an absolute temperature to within 10 K with the current state of temperature calibrations, which usually have an uncertainty of around 100 K. At this point we consider the fundamental physics and behavior of the temperature dependence of photospheric absorption lines, which is the core issue of the LDR method.

2.2 The Importance of Temperature

Temperature is an integral parameter in describing a photosphere (and is arguably the most basic of all stellar parameters). Effective temperature tells us what spectral type of star we are dealing with, and that classification allows us to make other inferences about the physical properties of the star, including mass, luminosity, radius, chemical composition, internal source of energy etc. Obtaining an absolute temperature scale requires continuum measurements and standard stars. One can measure the continuum of a star by comparing it with a standard star whose continuum energy distribution has been calibrated (Vega is the primary photometric standard for visible wavelengths. Secondary standards are calibrated to Vega.). Accurately fitting a stars continuum (or portions of it) is critical to the method of LDRs, as the depth is described by the distance from the continuum to the bottom of the line.

The primary variable in line strength is, big surprise, temperature. Most line strengths peak at a particular effective temperature. As temperature increases, excitation of a particular transition also increases; however, if the temperature continues to increase the transition in question may have a decrease in strength due to species ionization. We are considering a K1.5 dwarf star, which is relatively cool and compact (with a high surface gravity). These conditions produce a variety of atomic photospheric absorption lines.

For application to LDRs, we want to be able to predict whether the strength of a line is inversely or directly proportional to temperature change. Following Gray (1976) let us consider the visible region of a cool star where the opacity (κ_v)

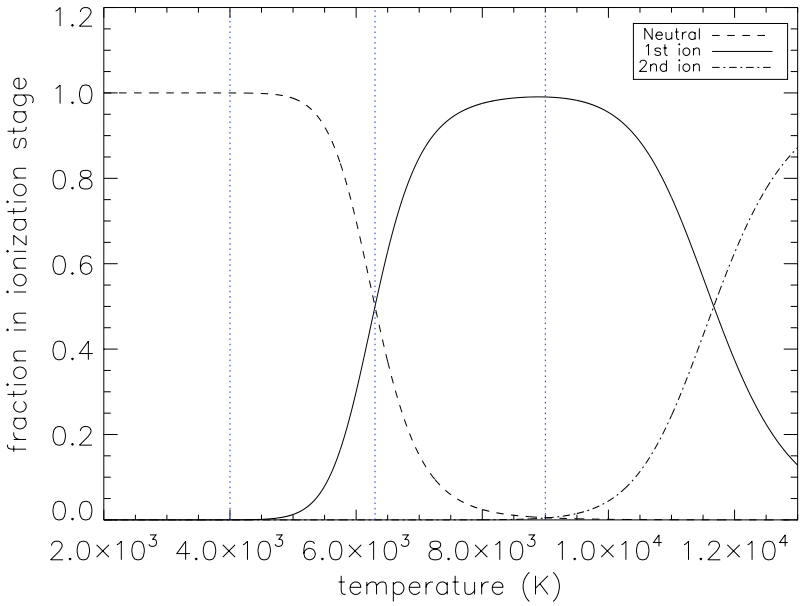

Figure 2.2: Ionization occurs fairly quickly with increasing temperature. The atoms we are examining exist primarily in the region indicated by the first blue dotted line. The second blue dotted line indicates where conditions 2) and 3) exist. The third dotted line indicates case 4), although in our analysis we do not use lines in first and second ionization states (in stellar photospheres elements usually exist in only two ionization stages).

can be approximated by the negative hydrogen ion's bound-free absorption.

$$\kappa_v = constant * T^{(-5/2)} P_e e^{(\frac{0.75}{kT})} \tag{2.1}$$

Where P_e is the electron pressure, k is the Boltzmann constant and T is the temperature in Kelvins. There are four sets of conditions worthy of attention: 1) weak mostly neutral neutral species, 2) weak mostly ionized neutral species, 3) weak mostly neutral ionic species, 4) weak mostly ionized ionic species. Their

respective temperature dependences are the following:

$$\frac{1}{R}\frac{dR}{dT} = \frac{2.5}{T} + \frac{X + 0.75}{kT^2} - \Omega T \tag{2.2}$$

$$\frac{1}{R}\frac{dR}{dT} = \frac{X + 0.75 - I}{kT^2} \tag{2.3}$$

$$\frac{1}{R}\frac{dR}{dT} = \frac{5}{T} + \frac{X + 0.75 + I}{kT^2} - 2\Omega \tag{2.4}$$

$$\frac{1}{R}\frac{dR}{dT} = \frac{2.5}{T} + \frac{X + 0.75}{kT^2} - \Omega \tag{2.5}$$

Where T is the temperature in the line-forming region, X is the excitation potential of the transition, Ω is related to electron pressure ($P_e = constant * e^{\Omega T}$) and is ~ 0.00117 for dwarf stars, R is the ratio of line to continuous absorption and I is intensity. Ultimately, the temperature of the line-forming region (which, according to Gray (1976), is about 15% lower than the effective temperature) and the excitation potential of the transition determine the direction and strength of the line change. The lines in our data set are described by the first equation. To give an intuitive sense of what these line dependences are, we consider the change in an FeI line of $X = 0eV$ and $X = 5eV$. Per 1000 K, the change in the FeI line with $X = 0eV$ is around -300%, whereas the change for the FeI line with $X = 5eV$ is about -100% (Gray 1976). The primary point to take away from all of this is that line strength depends on the sort of gas you are dealing with, the strength of line transitions and the temperature of the line-forming region (which is essentially the effective temperature). We are dealing with the first case: weak lines of a neutral species, with the element mostly neutral (Figure 2.2). You may notice that all four of these scenarios specify weak lines. Recall that saturated lines are not useful for LDRs because they are metallicity-dependent (their strength is also

a function of how much of that particular element is present in the star). For this reason, the lines that are most often and most successfully used in this method are weak metal lines.

2.3 Stellar Spectra and Line Depth Ratios

Spectral lines provide us with a wealth of information beyond the radial velocity of the star. Which spectral lines are present indicate the stellar metallicity, and the widths of lines place limits on stellar rotation rates. Spectral lines can also tell us something about effective temperature. In solar type stars, neutral metal lines are often the most useful because they have a wide range of temperature sensitivities but they are not pressure sensitive. Choosing lines that are nearly independent of stellar parameters (other than temperature) increases accuracy and efficacy of the LDR method. We consider VI, FeI, TiI, CrI, SiI and NiI lines in our study of temperature fluctuations in the exoplanet host star HD189733. In general the two lines being used should be relatively close to each other in wavelength to minimize continuum fit and normalization errors. Also, particular pairs of lines will only be useful within a particular temperature range, so determination of the strength and direction of the temperature dependence is important.

The most obvious downside to weak metal lines is that they are the most difficult to identify and measure because they are weak. They are also quite vulnerable to distortion by line-blending (when two lines occur at very close wavelengths, and the resolution of your data is not sufficient to tell one from the other). However, these issues are worth addressing because ultimately LDRs of weak metal lines increase observational precision and can indicate relative temperature changes on the order of 10 K or less (Gray 1994). Although you are assured of removing

any abundance dependence if lines of the same element are used (both FeI lines for instance) it is also reasonable to use lines from similar elements (Gray 1976). Gray (1994) cites Fe, V and Ti as similar, Kovtyukh et al. (2003) extend this and use Fe, V, Ti, Cr, Si and Ni with apparent success.

Chapter 3

Data/Observations

3.1 The Hobby-Eberly Telescope

The Hobby-Eberly Telescope (HET) is a 9.2-meter telescope located at McDonald Observatory in Texas. It contains 3 spectrographs that work at low, medium and high resolution. Our data were collected using the high-resolution spectrograph (HRS), which is located in a climate-controlled (∼0.3 K) basement below the telescope and fed by fiber optic cable. It can observe between 4000 and 10,000 Å with a resolution ($R = \frac{\lambda}{\Delta\lambda}$) ranging from 15,000 to 120,000 (Tull 1998).

HET was built to optimize cost with quality. One particularly interesting feature of the telescope design is that the primary mirror does not move to track the sky - the secondary mirror moves! It is a spherical telescope, so there is no preferred observational axis. This makes focusing and tracking rather complex, as the focal surface is also spherical. Eight tons of instruments (and the tracker) are located 13 meters above the primary mirror at the prime focus, and move across the face of the mirror to track objects. To accommodate the spherical focal surface, the tracker uses a six axis coordinate system to maintain focus while tracking. The whole process requires 10 different motors operating simultaneously. Objects can be followed for up to two hours. The primary mirror, like the 10-meter Keck telescopes, consists of (91) hexagonal pieces, which are much easier

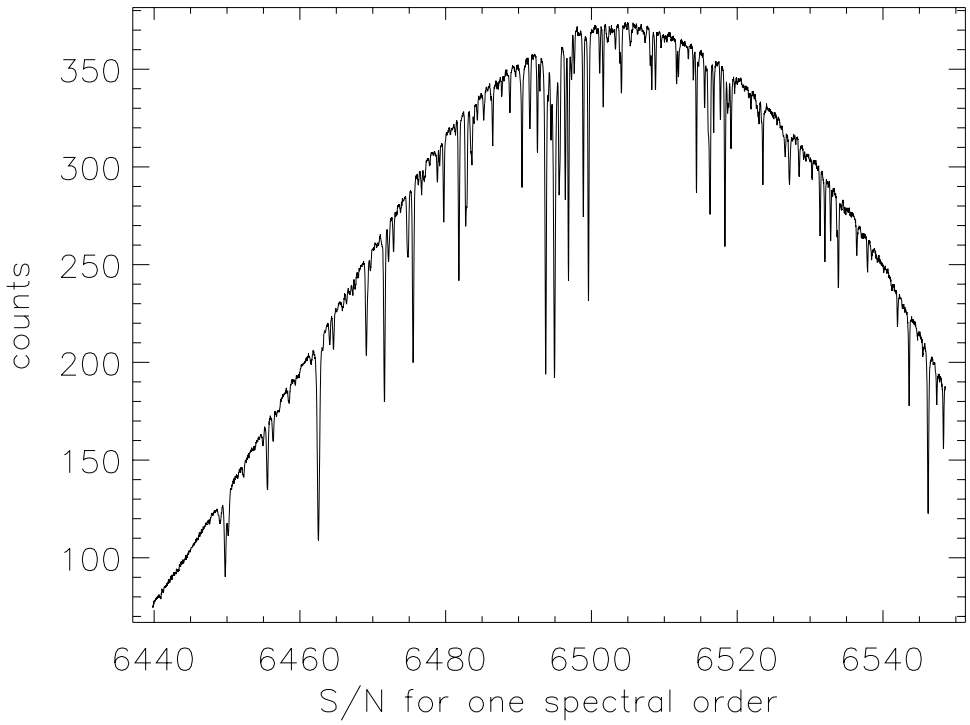

Figure 3.1: The Signal-to-noise ratio for one spectral order of the data.

to manufacture and work with than one huge mirror (Ramsey et al. 1998).

Observations at HET are queue based. This is especially good for transit observations, since transits do not take all night (usually they take a few hours) and only occur every week or so. The queue system is thus efficient at obtaining data for several different science projects on a single night, and also at collecting data routinely on non-consecutive nights.

3.2 Observations

HD189733 was observed as part of a large-scale program to look for excess absorption caused by an exoplantary atmosphere in the transmission spectrum (Redfield et al. 2008). Spectra for HD189733 were taken over 37 nights between August 11th 2006 and August 11th 2007 with the aforementioned high-resolution spectrograph. These observations occur both in and out of transit, have a resolution of about 60,000 and range between 5000 and 9000 Å. There are 11 in-transit visits (if the entire exposure is taken between first and fourth contact) and 25 out of transit visits. There are 204 exposures in total. The data were reduced using Image Reduction and Analysis Facility (IRAF) and Interactive Data Language (IDL) routines. For more details, see Redfield et al. (2008).

HD189733, like most cool stars, contains a wealth of photospheric lines. This is clearly evident in Figure 3.2. Figure 3.2 also shows that our spectra are not initially normalized and clearly bear the mark of a blaze function (a function determined by the spatial sensitivity of the detector). There are approximately 220 absorption lines per spectral order, and we have 204 exposures each containing 53 orders of spectra. This gives around 2.5 million potentially useful lines, which is more than sufficient for our investigation (I made these estimations by looking carefully at a 10 Å chunk of spectra and counting the number of absorption lines). As will become apparent, weeding through this bounty of lines and optimizing our line selection process is a large and important part of our work.

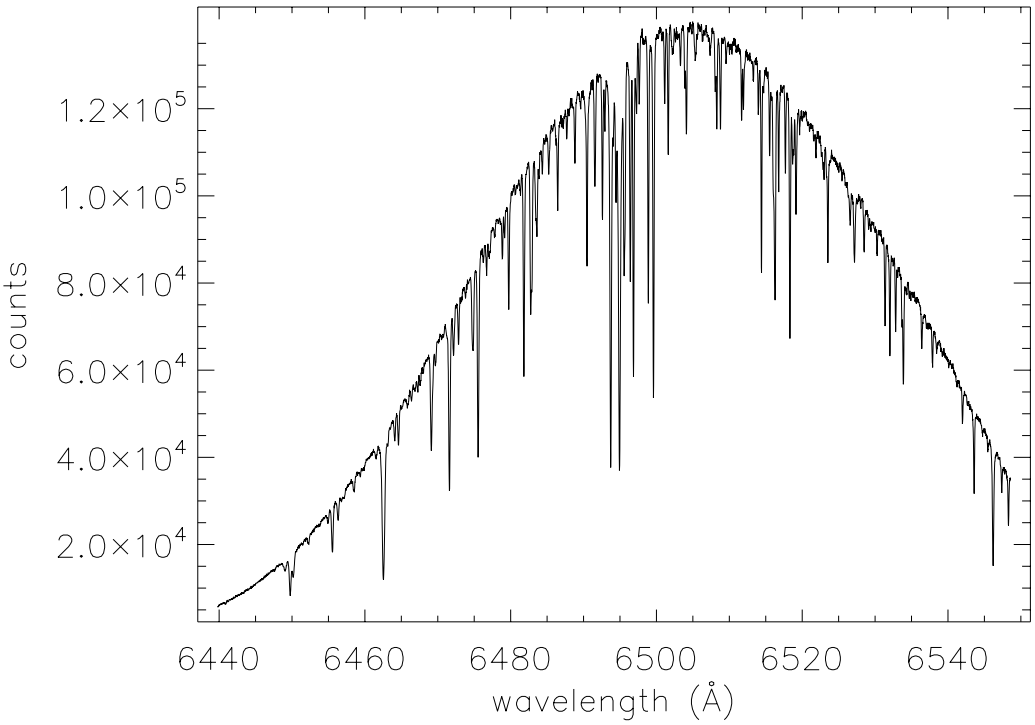

Figure 3.2: One spectral order of the data.

Chapter 4

Analysis

Our data set consists of 37 nights of observations taken over the course of a year. We have 204 echelle spectrograph exposures with wavelengths ranging from ∼5000 to ∼ 9000 Å.

There are a large number of photospheric absorption lines between 5000 and 9000 Å . We began our initial data assessment by choosing 6 neutral line transitions to consider: CrI, NiI, SiI, TiI, VI and FeI. These were chosen because they are temperature sensitive and fairly weak (to eliminate the possibility of saturation). We used the Kurucz line data base (Kurucz & Bell 1995) to build our initial line list that included 15,807 transitions of these atoms that might exist in our spectra.

We constructed a program to find and fit transitions from our initial line list in our data. In general, the goal was to go to the wavelength of a particular transition, and look to see if there was indeed an absorption feature at that wavelength. If the program was able to fit a Gaussian to a feature at this location, then it also applied an iterative series of polynomial fits to the continuum within ± 3Å of the feature. The initial fit to the continuum was linear and was applied to the data set in the bracketed 6-Å range (Figure 4.1).

Any points below the first fit (presumably those points in the absorption feature) were discarded. A second linear fit was performed on the remaining points, and again those below the fit were discarded. The third and fourth fits were both

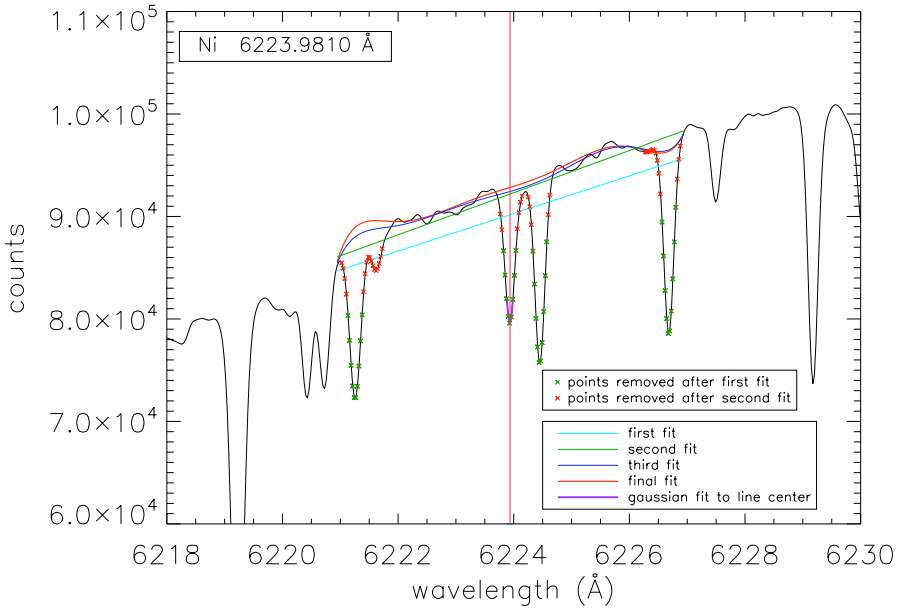

Figure 4.1: An example of our continuum fit.

of order 7. The fourth fit is what we kept as the best fit to our continuum. We normalized the region in question by dividing the actual data by the fit to the continuum (Figure 4.2). It should be noted that prior to the 6 Å window we attempted to do the continuum fit within a much smaller range around the possible absorption feature, but this was less effective than the longer baseline approach.

Obtaining a good continuum fit is a critical part of measuring line depths. Our line depths were measured off the normalized plot. The blue line in Figure 4.2 is a gaussian fit to the line of interest (whose wavelength is indicated by the red vertical line). We defined depth to be the distance between the continuum value (1 on the normalized plot) and the bottom most point of the gaussian fit.

The data were fit, sorted and analyzed with a series of IDL programs. It is

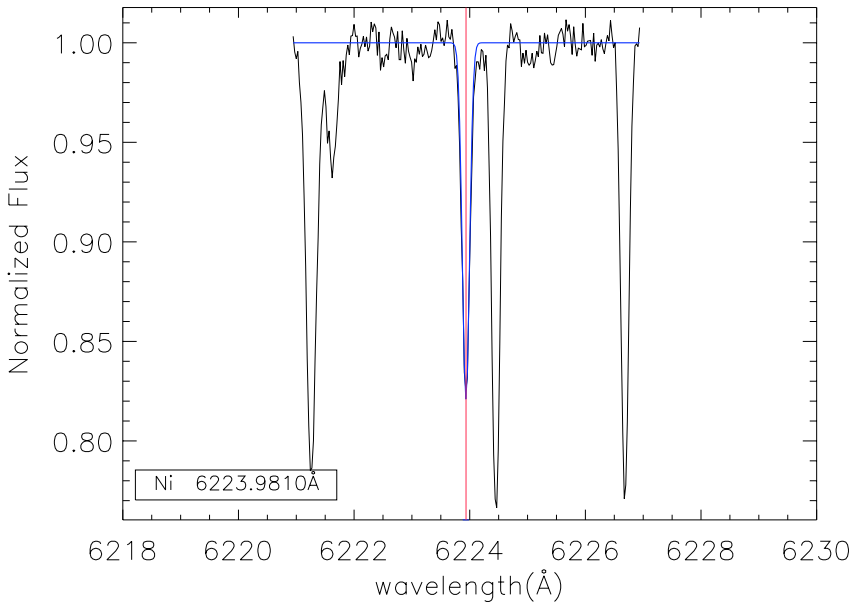

Figure 4.2: An example of continuum normalization. Our line depth measurements were made using the normalized spectra.

useful to consider the programs and outfiles in the order they were created and used to more easily follow the progression (see the following flow charts).

4.1 Data Process

This section is best read while following flow chart 1.

Transitions having exactly the same transition wavelength in the aforementioned input file were eliminated because there was no way to determine which line was actually present in the data. For example, there is a CrI line and a VI line that both occur at 5025.553 Å . These exact duplicates were removed. Lines that were within .005 Å of each other were also removed as the resolution of our

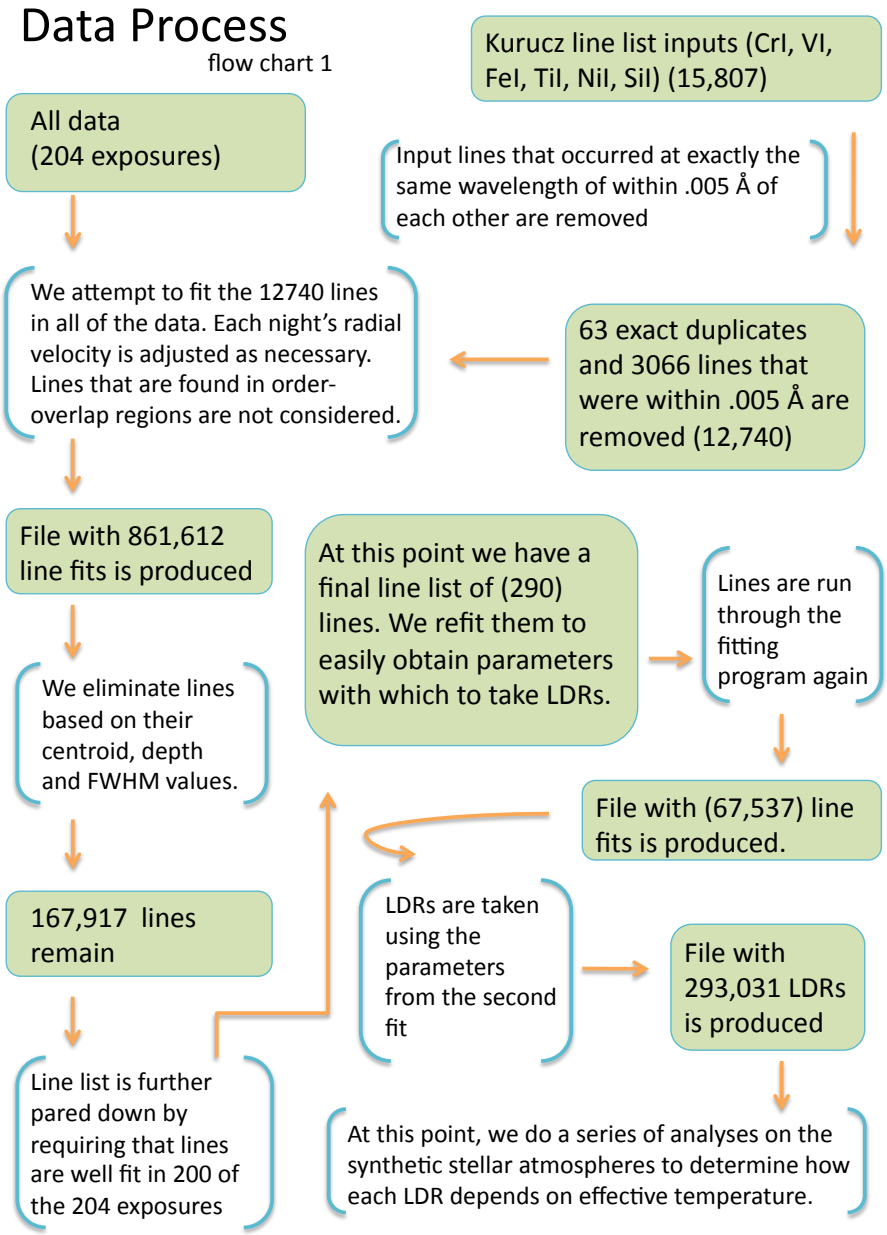

Figure 4.3: Flow Chart 1: A progression of the data analysis.

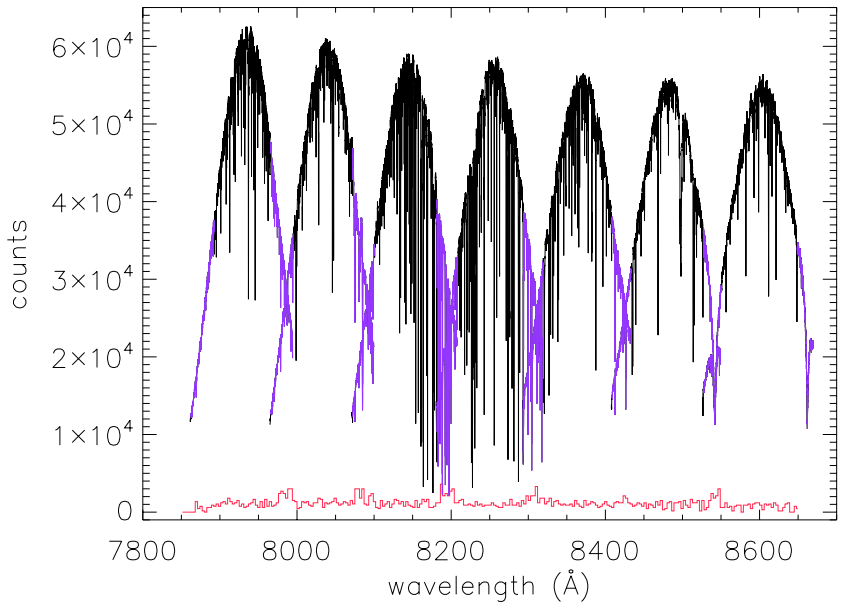

Figure 4.4: The purple region indicates overlapping parts of spectral orders, and the pink histogram on the bottom is a histogram of all the lines that were fit in within those wavelength ranges, scaled up by a factor of 150 so that it could be put meaningfully on this plot. You can clearly see a periodic rise in the histogram, which corresponds to the regions of order overlap. This confirms that we were initially fitting lines in multiple orders. As discussed, these purple regions were ultimately removed from consideration.

data would not allow us to distinguish between such close inputs.

After these cuts were made, the truncated list of input lines was fed into a continuum fitting program that simultaneously did several calculations: Firstly, it located where the line, if present, should occur. If found, it determined whether or not the line was in a region where the echelle spectral orders did not overlap. The blaze function made it difficult to measure comparable line depths of lines that were fit in multiple orders, so we eliminated those regions from consideration (Figure 4.4).

Then, if the line was in a non-overlap region, it fit the line with a gaussian and the continuum with an iterative series of polynomial fits ranging from linear up to order 7 (as mentioned before). This program also adjusted the resolution of the spectra. The data were collected over the course of a year, and so the resolution of the instrument varied night to night. Line depths take up a constant area and the resolution of the data determines how broad or narrow the lines are, so resolution variations are important to correct for when accurate line depth measurements are necessary (Figure 4.6). Resolution variation is mostly caused by the difficulties associated with keeping the instruments at cryogenically cool temperatures (Figure 4.5). This is more of a challenge in the summer than the winter, for obvious reasons. We compensated for this by adjusting the resolution of all the data to a resolution slightly lower than the worst night (R $\sim$ 50,000).

The large quantity of output from the initial fitting program was pared down using a series of cuts on the centroid values of the line fits, line depths and full-width half-maximum (FWHM) values. The centroid values of true lines were extremely close to zero because of the way the fit program re-centered itself on each line in question (see Figure 4.7). The fact that the centroid distributions are tightly centered on zero is an indication that our radial velocity values for each night of observations are sufficiently accurate.

Lines with positive depths were discarded (positive depth generally indicated that a bump in the continuum noise had been fit erroneously) as were depths greater than -1 (the depths were measured from the normalized plot, so a value of -1 clearly indicates some error), as were lines with FWHM values that exceeded one Å. This FWHM cut eliminated situations in which severe line blending caused the fit algorithm to proceed as though a line was present, when really a group of indistinguishably blended lines were present. We were unable to use these

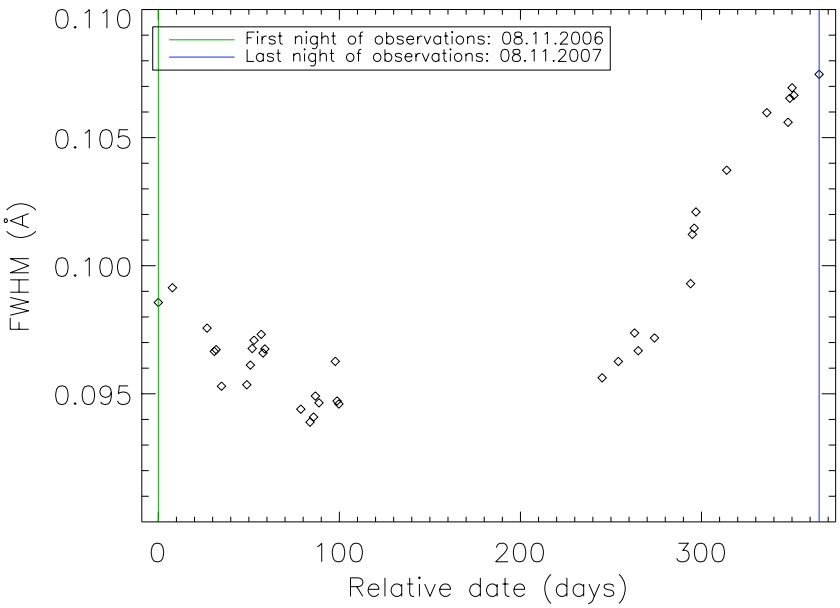

Figure 4.5: Nightly variation in the data's resolution.

extreme blends because it was impossible to determine with certainty which line was actually in the data.

Output from the centroid cut was then fed into another program that made a cut based on how frequently a line was successfully fit in the data. Recall that the data consist of 204 exposures made over the course of one year. Thus, a line that is assuredly present in the spectrum should be fit 204 times. We selected 872 lines that occurred 200 times or more (Figure 4.10).

The remaining set of lines was put through another fit routine identical to the first fit routine to conveniently produce line depth measurements. After being fit for a second time, line depth ratios were taken. We required the lines used to calculate LDRs be from the same night and the same echelle order to reduce con-

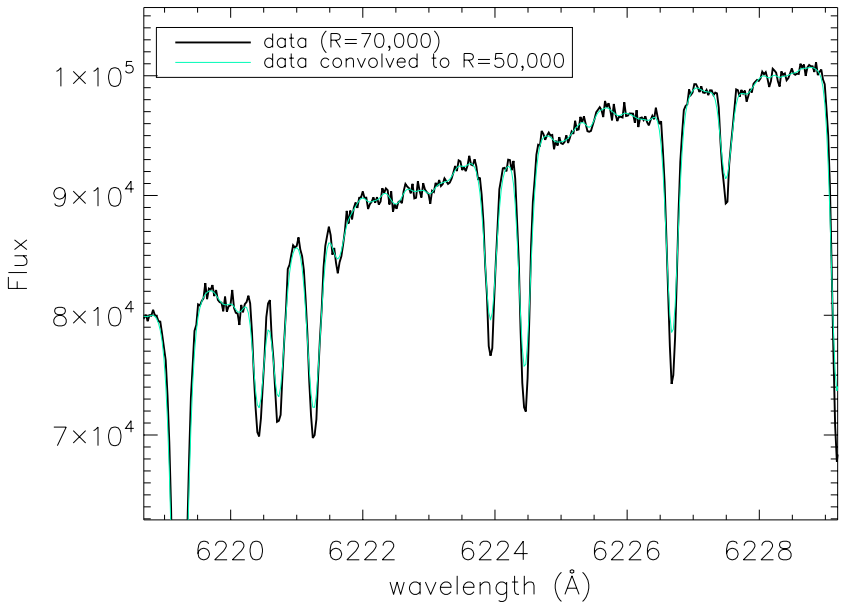

Figure 4.6: An example of how the convolution affected the data. As expected, adjusting the resolution of the data down to a common level caused the absorption line depths to be a bit shallower. Since precise line depth measurements is paramount for our analysis, this was an important step to get right!

tinuum measurement errors and other systematic sources of error, including those that might be wavelength dependent, and those associated with data reduction tasks (like flat fielding).

Nearly 300,000 LDRs were produced using this method. Using our synthetic stellar atmospheres (to be discussed in the next section), we determined the strength of the temperature dependence of each LDR, and selected only those with significant temperature dependence.

Ultimately, our goal is a plot of effective temperature vs time. As an intermediate step, it is useful to create LDR vs time plots. To do this there is some

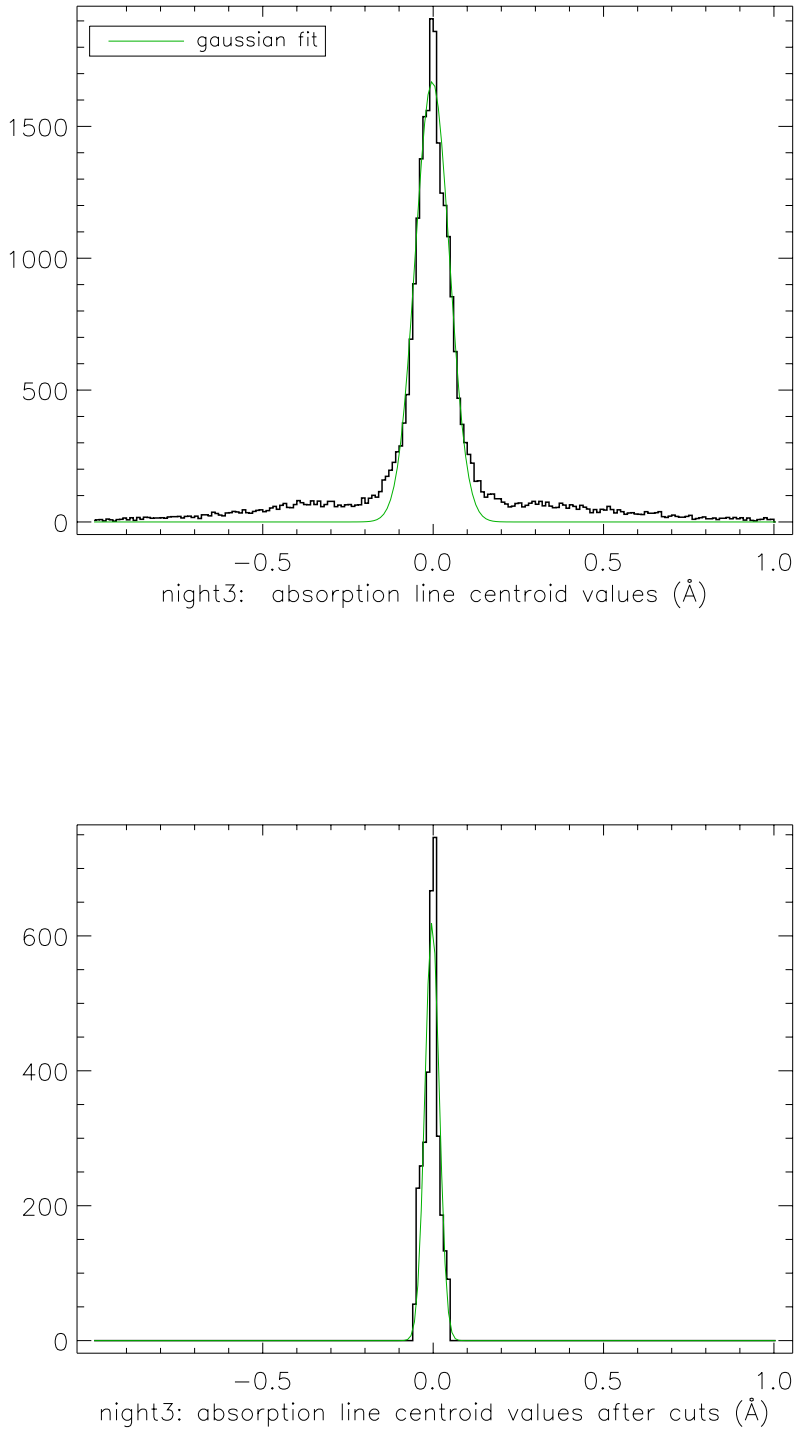

Figure 4.7: Histogram of all calculated centroid values and then the centroid values after the centroid, depth, and FWHM cuts for one night of observations.

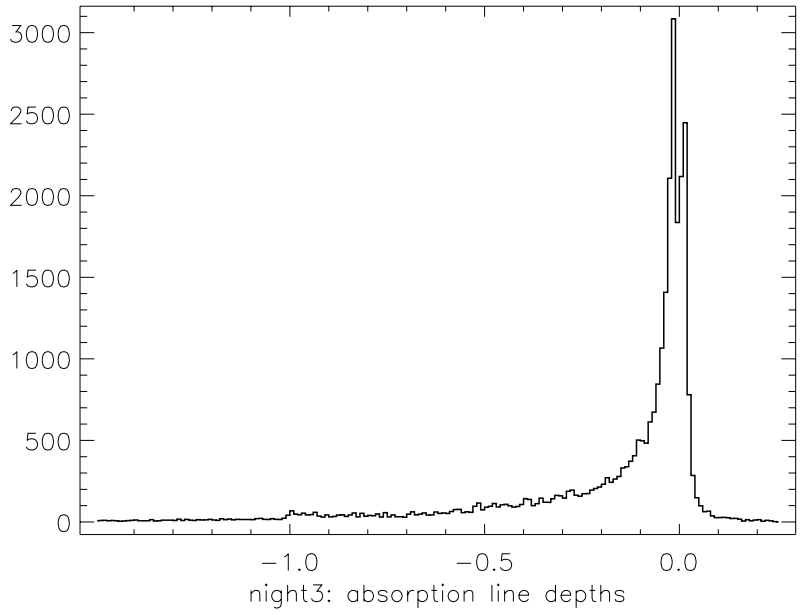

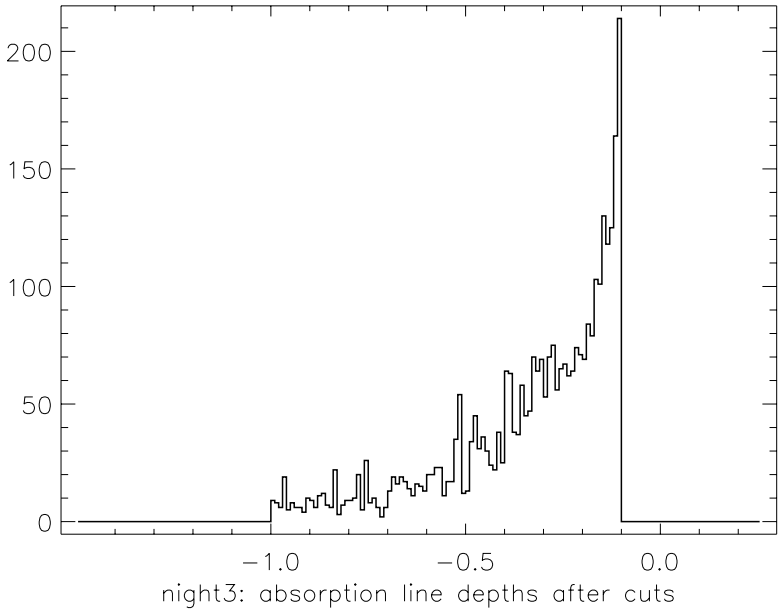

Figure 4.8: Histogram of depth values for one night of observations.

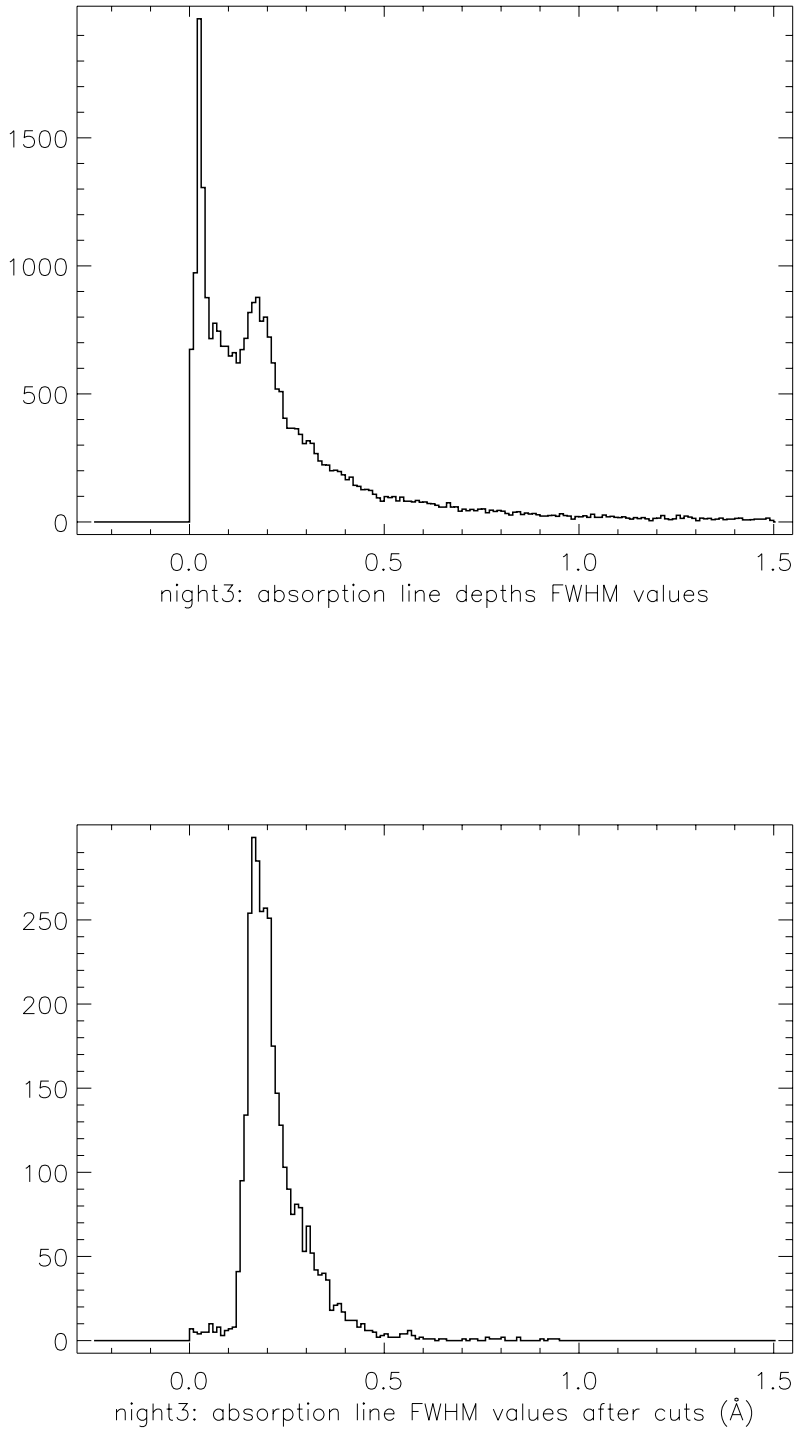

Figure 4.9: Histogram of FWHM values for one night of observations.

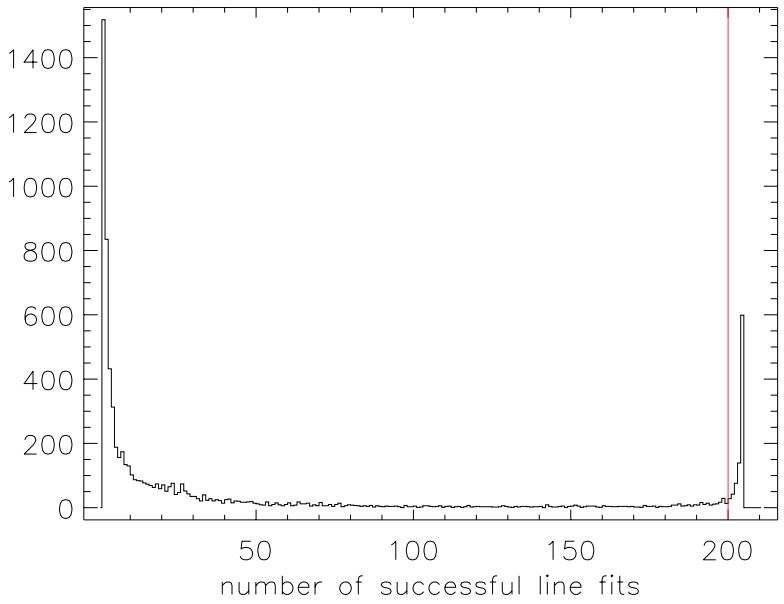

Figure 4.10: Lines that were fit consistently in every exposure are very likely to be real lines. We only used lines that occurred in 200 out of the 204 exposures (98%). The spike at zero indicates that many of the lines in our initial list were fit only once or twice in the entire data set, indicating that there was coincidentally a feature in the data that the program could fit, but the line was not actually present.

housekeeping that has to be done to match up LDRs with the Julian date of the night of observations.

4.2 Model Process

Our model spectra were constructed specifically for K dwarfs at a variety of effective temperatures ranging from 4620K to 5260K by Lars Koesterke (Koesterke et al. 2008). They are extremely high resolution (R $\sim$ 120,000) and utilize the Kurucz line data base (Kurucz & Bell 1995). We actually degraded the resolu-

tion of the models down to the degraded resolution of the data (R = 50,000) to ensure that all the parallel processing of the data and the models was completely analogous.

Much of the computation done on the models is similar to that done on the data. Significant differences include that the model spectra were already normalized. We therefore assume that our errors in continuum and depth fits are negligible.

The primary functions of the models were to provide a check that the lines we found and fit in the data were reasonable, and to create a calibration between line depth ratio and temperature. We did this by using 33 models at different temperatures from 4640 K to 5260 K. Our final line list (obtained from our data) was fit in every model and as in the data processing, the resulting line list was run through the same series of centroid, height and fwhm cuts and then refit a second time to facilitate taking ratio measurements. This secondary implementation of the centroid, height and FWHM cuts are done to ensure that any rogue line that might have made it through the data processing got eliminated in the model processing. An especially nice feature of the models is that they are based on the Kurucz line data base, and they are at rest wavelengths. Thus the radial velocity shifts that had to be determined for each night of the data are not necessary here. In retrospect, this really should have been the first step in eliminating irrelevant lines, but that is a discussion for another section. LDRs were then taken between all lines within the wavelength range of the data orders, and LDR vs temperature plots were thereby readily obtained.

The list of LDRs was reduced, and the temperature dependence of each individual LDR assessed by plotting the LDRs vs temperature and doing a linear fit to the data. As can be seen in Figure 4.12, many of these LDR-temperature

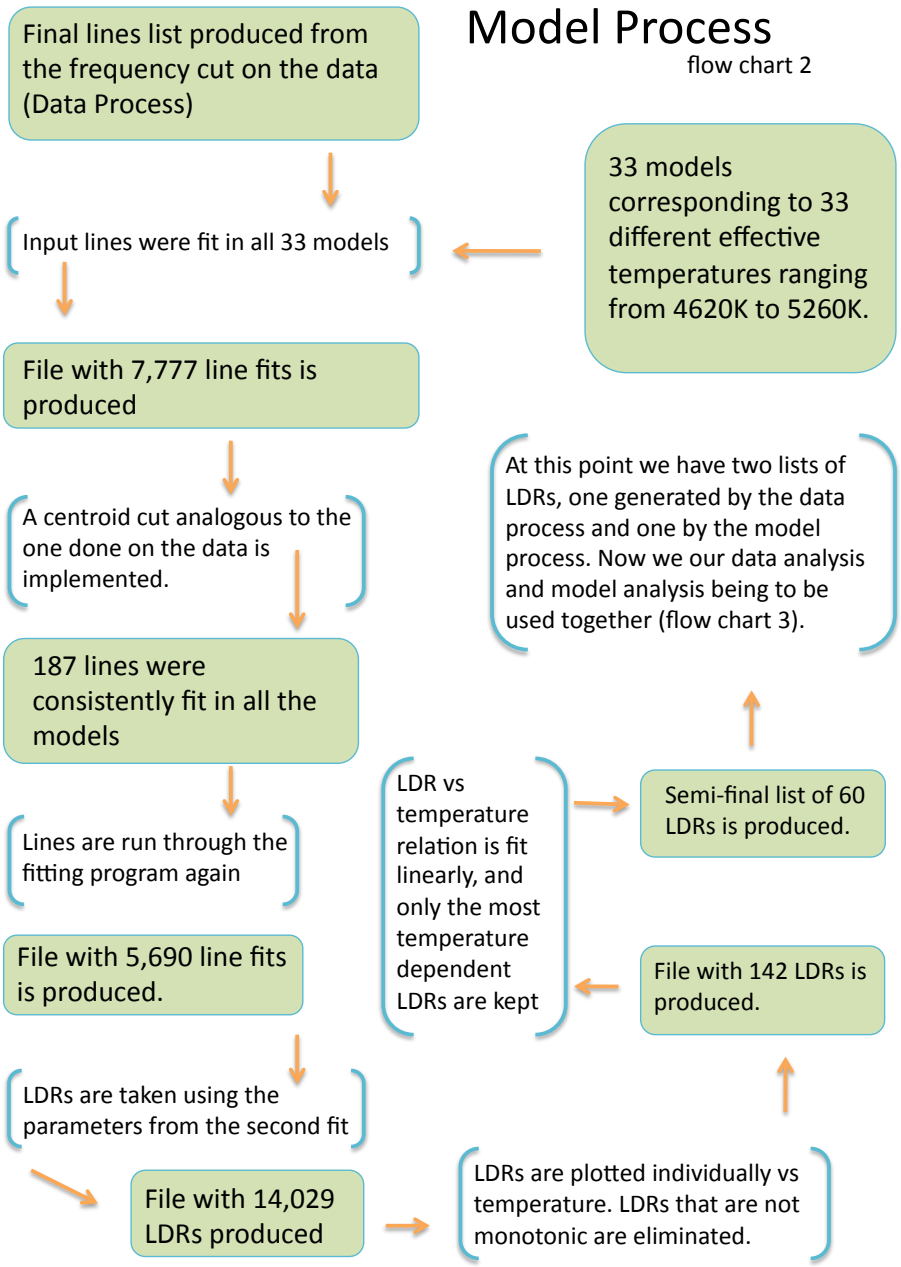

Figure 4.11: Flow Chart 2: A progression of the model analysis.

relationships are strong and linear.

4.3 Combining the Data and Models

At this point we have two sets of LDR lists (4.13) from the model processing and the data processing. These two lists define a final list of LDRs and the dates that they were measured on. At this point we are able to look at LDR vs time plots.

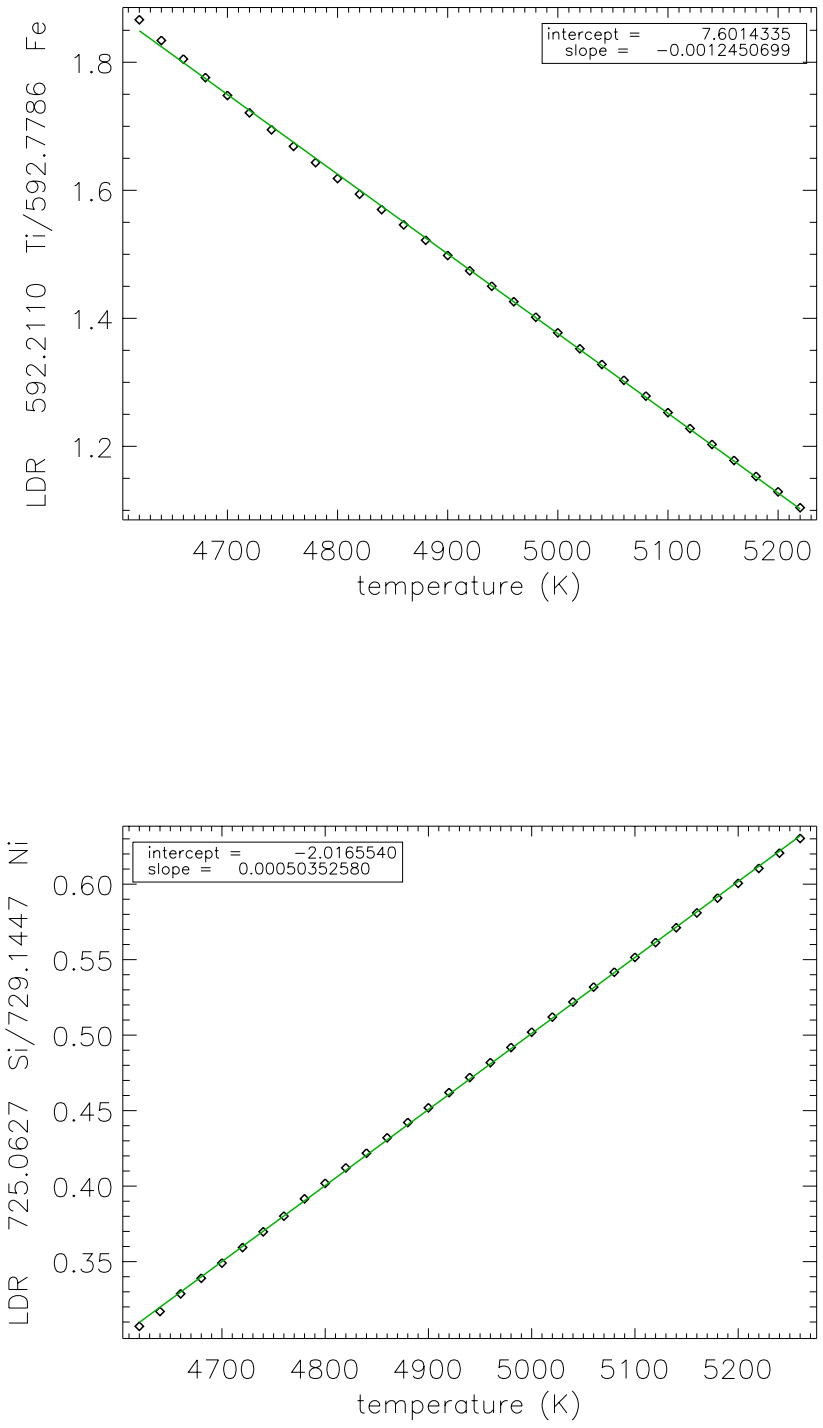

Figure 4.12: The temperature sensitivity of two LDRs.

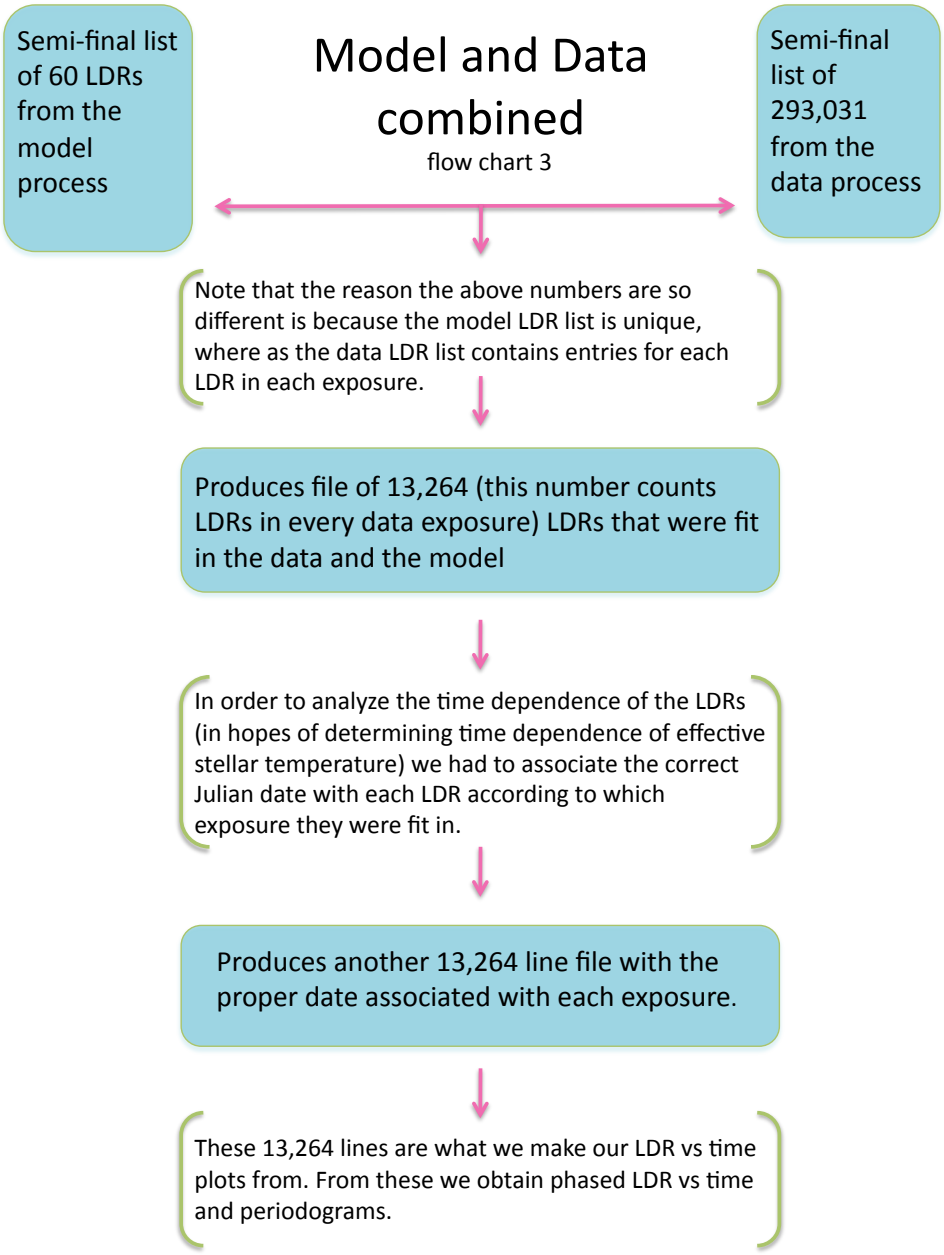

Figure 4.13: Flow Chart 3: Using results from the model process and the data process to arrive at LDRs vs date, phase-folded LDR curves and periodograms.

Chapter 5

Results

5.1 Goals

Although this section is primarily about what we have produced, it is helpful to have some idea of what the best-case scenario goals were, so that how close (or not so close) we came to achieving them can be clearly illustrated. The ultimate dream case would have been to obtain effective temperature vs time plots that indicated stellar variability on the timescale of the star's rotation period and/or the planet's orbital period. I would not have to include a separate 'Goals' section if all of them had been realized. However, articulating the big picture in this project's particular case does illustrate how close we are to either achieving our 'best-case' goals, or concluding that our particular methods are not an effective way to fit and analyze LDRs.

5.2 Results

At this point, we have produced LDR vs time plots. Recall from the previous section that LDRs are a great proxy for relative temperature change, and we have identified several temperature dependent LDRs, functionally fit their temperature dependence and produced LDR vs temperature vs time plots (Figure 5.3).

Notable in particular about Figure 5.3 is the inverse shape of the trends: the

top LDR decreases with increasing temperature, while the LDR in the bottom plot increases with increasing temperature (this is consistent with what we illustrated in Figure 4.12). Thus, for a given temperature change, the LDRs should exhibit opposite behaviors, which the two examples in Figure 5.3 clearly do. Based on these cases, we might infer that for the 10 days over which the LDRs are plotted, HD189733's effective temperature initially decreases and then begins to rise again.

We have also phase-folded some of our temporal LDR results, looking for periods on the timescale of the planet's orbit (2.2185733 days) and the stellar rotation period (11,953 days) (Henry & Winn 2008). There is at least one case that looks like it might contain some sort of signal (Figure 5.5).

Besides this narrow view at the very end of the process, it is worth noting that although our final set of results are not yet polished or conclusive, along the way several important developments have occurred. We have designed an effective spectral fitting program that is capable of adjusting the resolution of the data, identifying a particular spectral line (even if the data is not adjusted for radial velocity shifts), fitting the continuum reliably and consistently, normalizing the portion that was fit and returning parameters relevant to the fit and input data. This process took about a year to perfect. Months were spent developing and revising a fit program that could be automated on a broad and diverse data set.

We also identified a number of unexpected obstacles and devised ways to avoid them or accommodate them. One example of this is the resolution adjustment of each night of data based on the resolution of the thorium-argon lamp that day. During the summer months in particular the resolution of the instrument was slightly lower than during the winter due to the difficulties associated with maintaining cryogenically cold conditions in the middle of a Texas summer. Because spectral lines take up a constant area, the resolution of the data has a significant

effect on the measured line depth. Adjusting all the data and the models down to a common resolution was an important step in measuring accurate line depths.

The overlapping of the (echelle) spectral orders created another set of challenges to our particular project. The blaze function of the spectrograph describes the relative intensity of incoming light as a function of wavelength in each order. Thus lines fit in different places in different orders are not comparable without calibrating the blaze function, which we did not do. Instead, we excluded any order overlap regions from our consideration. This sounds simplistic here, but it took quite some time to correlate oddities in our LDRs with this order overlap.

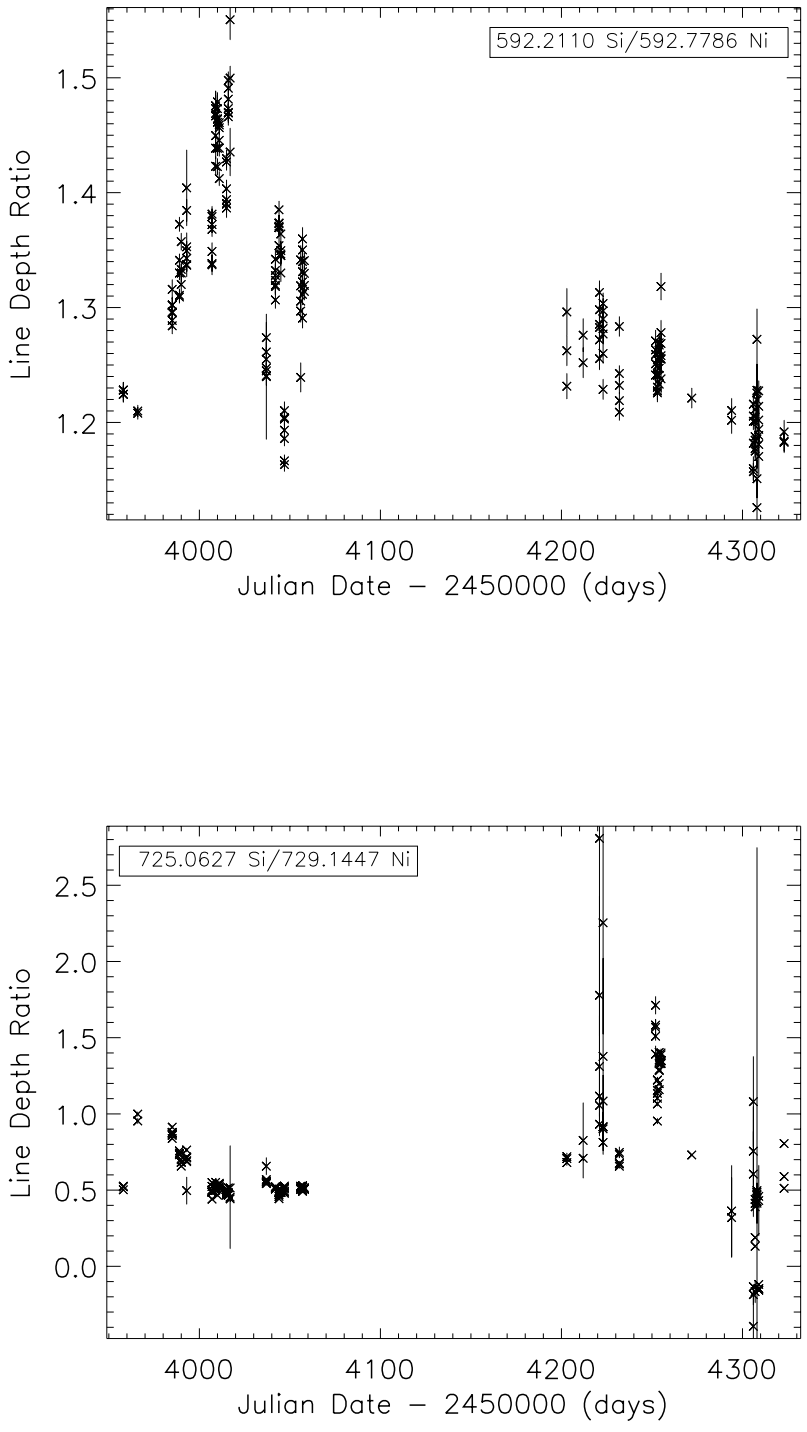

Figure 5.1: A LDR plotted vs time for the entire data set.

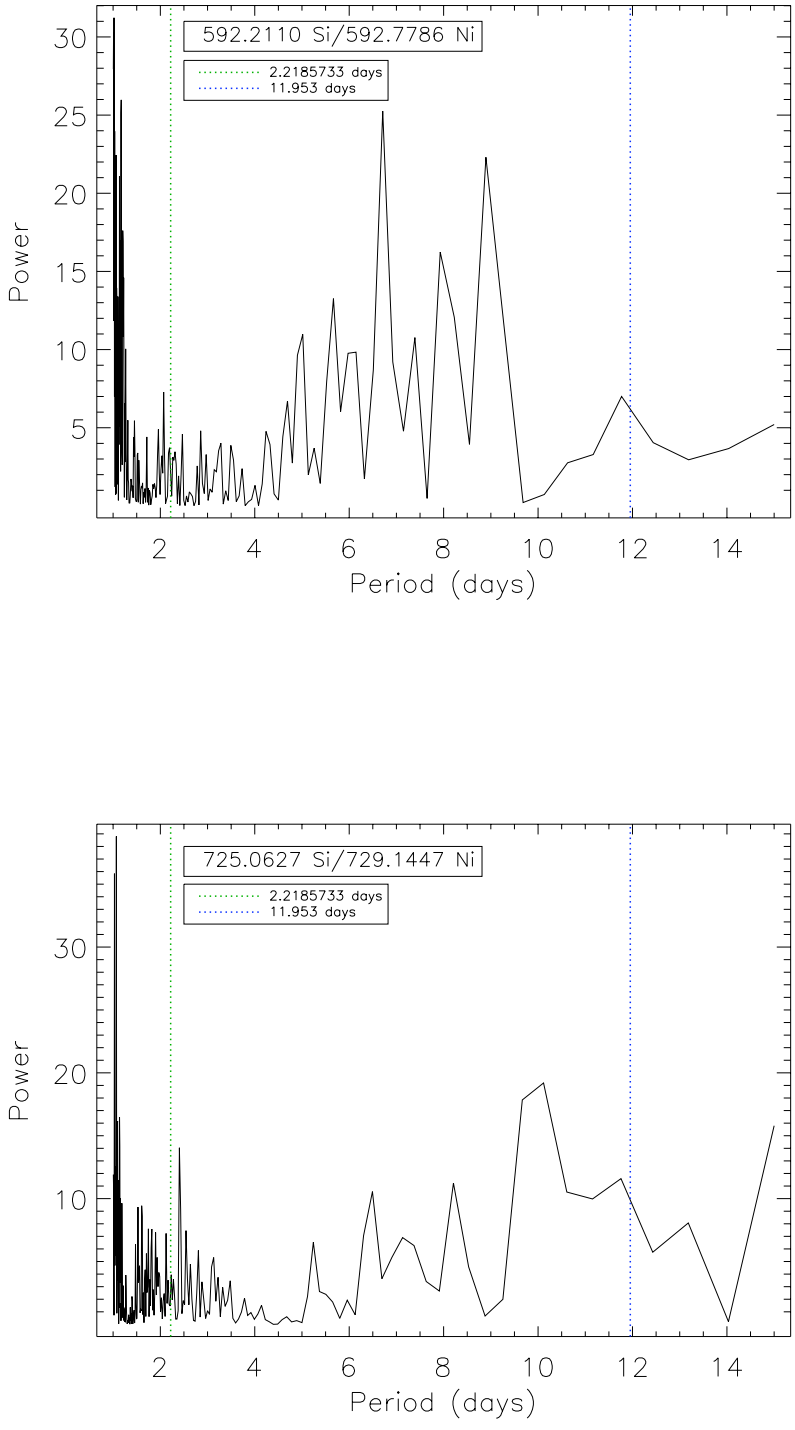

Figure 5.2: A periodogram of the LDRs in 5.1 using data from all the observations.

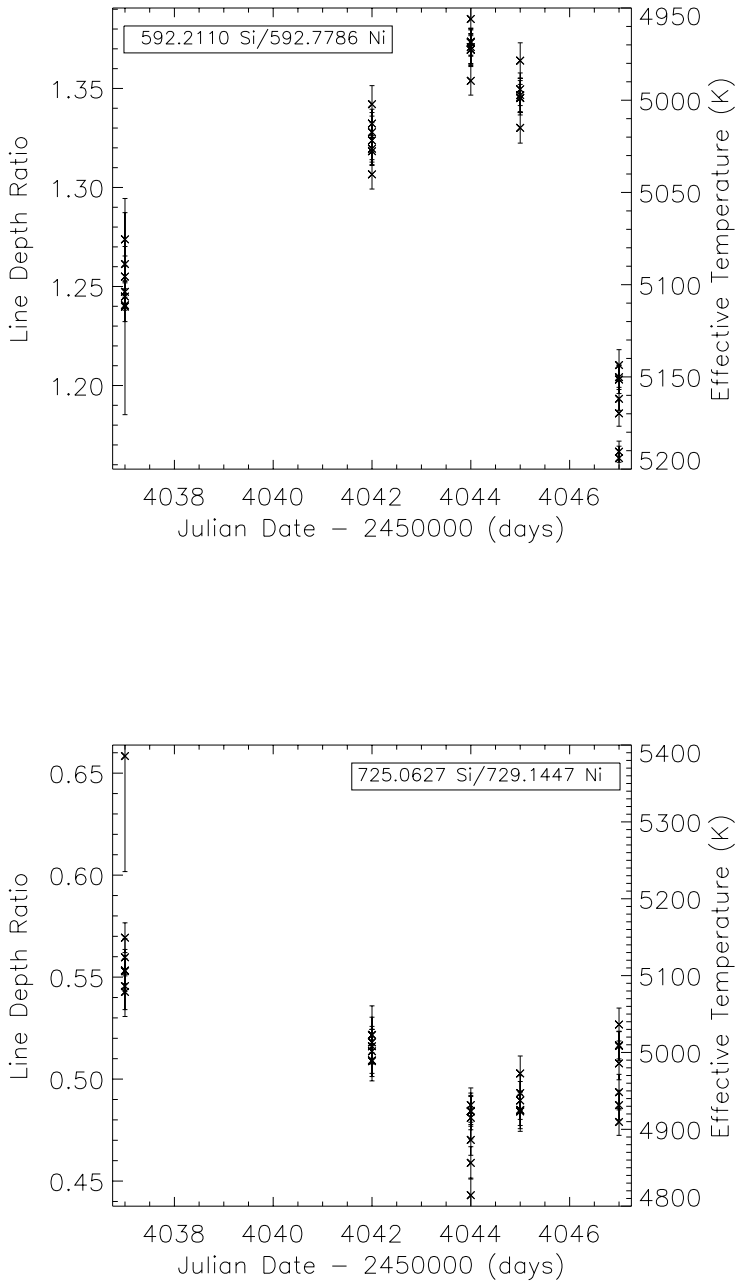

Figure 5.3: Two LDRs were plotted vs date for a subsection of the data set (about 10 days). Because HD189733 is such an active star, it is useful to plot LDRs vs time for subsections of the data to look for periodicity. Short term periodicity, because star spots form and disappear so quickly, could be impossible to find if we consider the data set only as a whole. Note the opposite behavior of the LDRs. This is exactly what we expect from two LDRs with opposite temperature dependences.

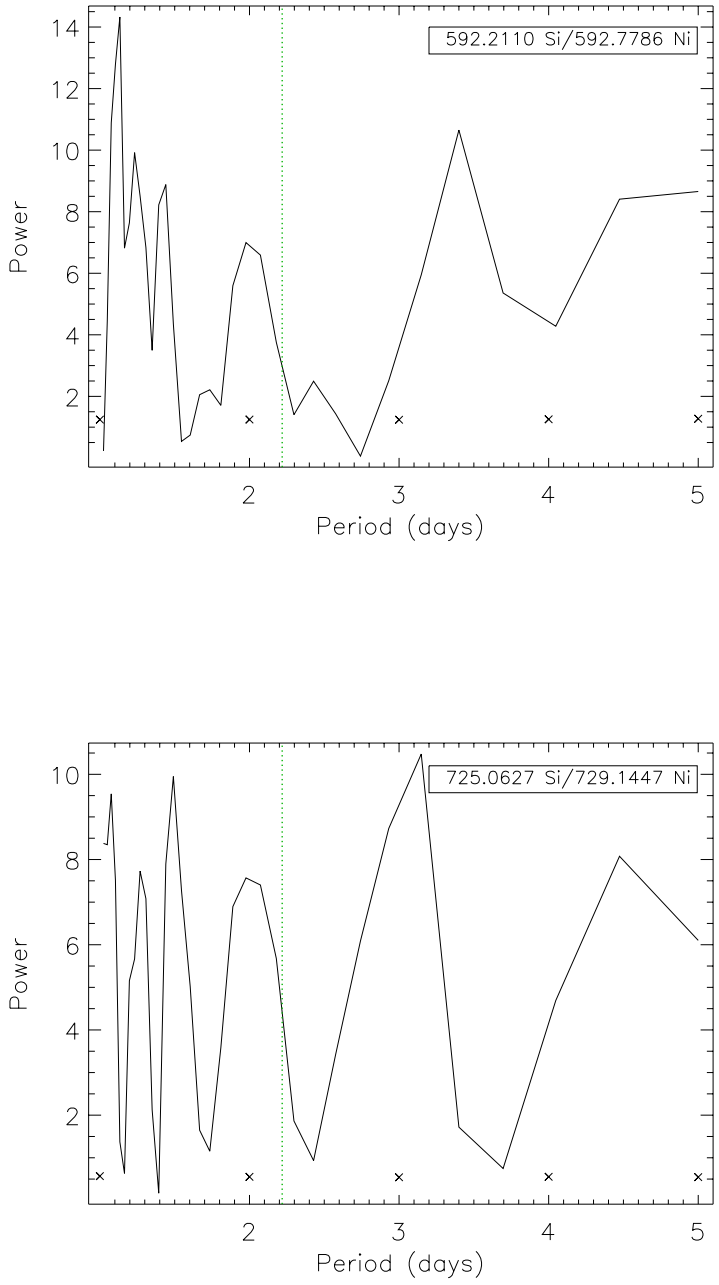

Figure 5.4: Periodogram of the LDRs in Figure 5.1 using data from the 10 day subset considered in 5.3. Although we phased the data during this time period with the 11.953 day period, it did not make sense to try to periodogram a subset of data for periods longer than the data subset.

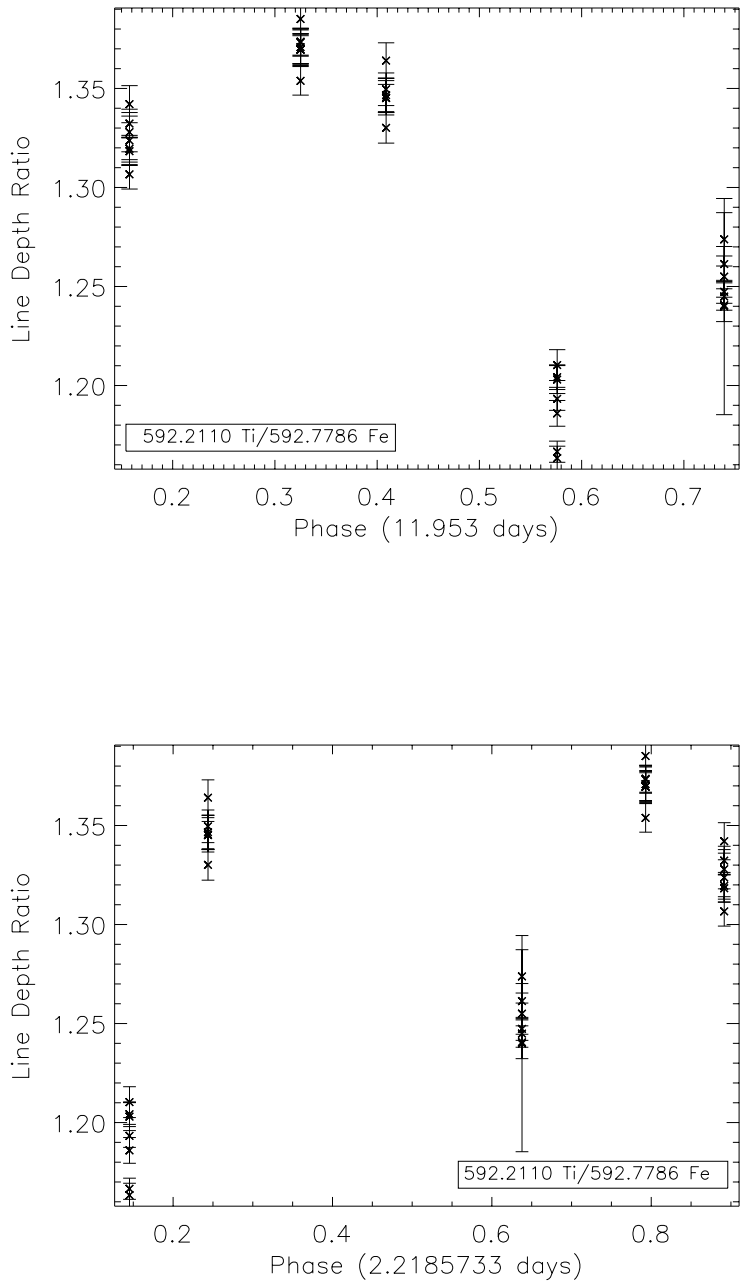

Figure 5.5: Data phase-folded at the stellar rotation period (11.953 days, top plot) and the planet's orbital period (2.2185733 days, bottom plot) for one LDR. The optimist may see a sinusoidal shape in the top plot. A clear, full sinusoid would indicate that the data has a strong variation with a period of 11.953 days.

Chapter 6

Conclusions

Conclusions are a tricky thing to make. This project has certainly not been mined to its full potential. Yet there are some statements that might be made regarding the effective temperature variations of this exoplanet's host star. Figures 5.3 and 5.5 certainly indicate stellar variability. Those plots, and what previous research has revealed about HD189733, seem like more than enough basis to conclude that HD189733 is a highly active star. We can also tentatively conclude that the variability is periodic on the time scale of the stellar rotation, based on Figure 5.5, and is likely due to stellar spots. This conclusion is a fairly safe one to make as variation due to spots in this system was suggested by Henry & Winn (2008).

We knew this data set contained a huge amount of spectra. Now we have confirmed that the spectra contains hundreds of temperature sensitive absorption lines that can be used in LDR analysis, which may prove to be invaluable in future research as increasing relative temperature sensitivity is required to see phenomena as weak and distant as planet star interactions in exoplanetary systems.

Many groups have observed HD189733 because it is relatively nearby and contains a relatively large planet. Henry & Winn (2008) identified the 11.953 day stellar rotation period during observing seasons 2005-2007 by monitoring the effects of stellar spots, and we see some evidence that we also detect periodicity

on this timescale (Figure 5.5). Our data was taken between August 2006 and August 2007, so there is significant (if not total) overlap between the dates of our data set and the dates of Henry & Winn (2008). Although we do not yet see any convincing periodicity on the timescale of the planetary orbit, there are several improvements to our method that we will be implementing in our future work.

6.1 Future Work

Our work is, at least conceptually, pretty much cut out for us from here. We have an enormous quantity of data - we will take advantage of this by normalizing our LDR to temperature relations and co-adding them. This will require careful functional fitting of each LDR's temperature dependence and mapping of all the LDRs to temperature.

As previously mentioned, this project is not complete. In retrospect, as we move forward, we may consider doing a few things differently. Instead of beginning with fitting the Kurucz line list in the data, we will fit the list in the models first. This will help us more definitively identify which lines are likely to be present in our data earlier on in the process. It will also be more reliable because the models are built on Kurucz model lines at rest wavelengths, and the initial line list contains Kurucz's rest wavelength values for the transitions in consideration.

We will also analyze the data in several subsets as we did in Figure 5.3. At the AAS meeting we were fortunate enough to have insightful conversations with Eugenia Shkolnik, and she pointed out that the rate of variability of HD189733 is so high that phasing and periodograming across the entire data set may actually smear out periodicities that vary slightly. For example, the stellar rotation period as derived from stellar spots by Henry & Winn (2008) may be 11.953 days for

dates spanning 2005-2007, but it may be slightly different if one considers only one year of their data or data taken during a different year.

As mentioned earlier, the sub-field of astronomy that deals with exoplanets and their host stars is new and growing. There are so many aspects of exoplanets that technology is allowing us to study. Already high resolution spectroscopy (of this data set!) has revealed that HD189733b's atmosphere contains sodium (Redfield et al. 2008). Studying the composition of exoplanetary atmospheres is exciting in and of itself, but it also could have implications for life in the universe. Chemical biosignatures may yet be detected in the atmospheres of planets. This is more dependent on extremely high resolution spectroscopy and line identification than LDRs, but our work has certainly made steps towards careful analysis of high resolution spectra.

Another issue directly related to the HD189733 system is the high stellar activity of low mass dwarf stars. Low mass stars are by far the most abundant in the universe because they require less material to form and then live orders of magnitude longer than higher mass stars. Thus, if they turn out to contain a habitable zone, looking for planets around them would be an endeavor worth undertaking. A habitable zone is defined to be the range in distance from a star where the temperatures are such that liquid water might exist. This is in fact already being done with the M-Earth survey Charbonneau et al. (2008), which has confirmed at least one exoplanet around a nearby M-dwarf star. There are several aspects of M-dwarfs that call into question the viability of a truly habitable zone, including the small size of the zone itself, its close proximity to the host star (planets are often tidally locked to the host star in these systems) and their high magnetic activity. There is some evidence that M-dwarf planets may be x-ray fried by their hosts. However, there is also evidence that this irradiation may not

be the quandary it appears - planets may also have strong magnetic fields, novel radiation defenses and other features that we have not thought of or observed yet. In any case, LDRs will be an invaluable resource in assessing the variability of M-dwarf stars! Because their effective temperatures vary so quickly and star spots form and dissipate on such short time scales, high resolution methods like LDRs are going to be required if we are to have any chance of figuring out what is powering their dynamo and how the activity is affecting the star's immediate environs.

These are just a few of the exciting on-going research fields that are related to high resolution spectroscopy (and therefore LDRs) and exoplanets. There are assuredly many more! It is an exciting time to be an astronomer.

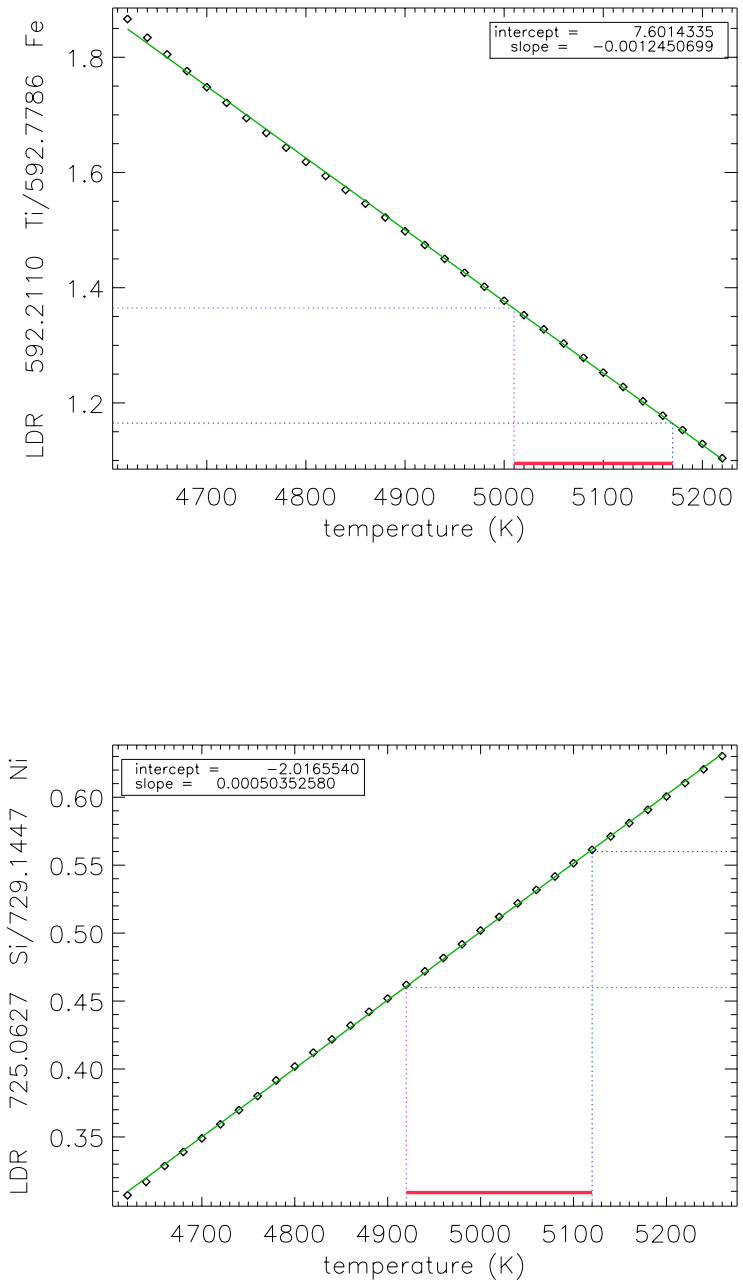

Figure 6.1: These are the monotonic plots from Figure 4.12 with the temperature range (pink) corresponding to the ratios (with the exception of one outlying point) from Figure 5.3. The temperature ranges indicated by the two ratios do not exactly match, as we would hope, but they do overlap, which is encouraging for our future analyses.

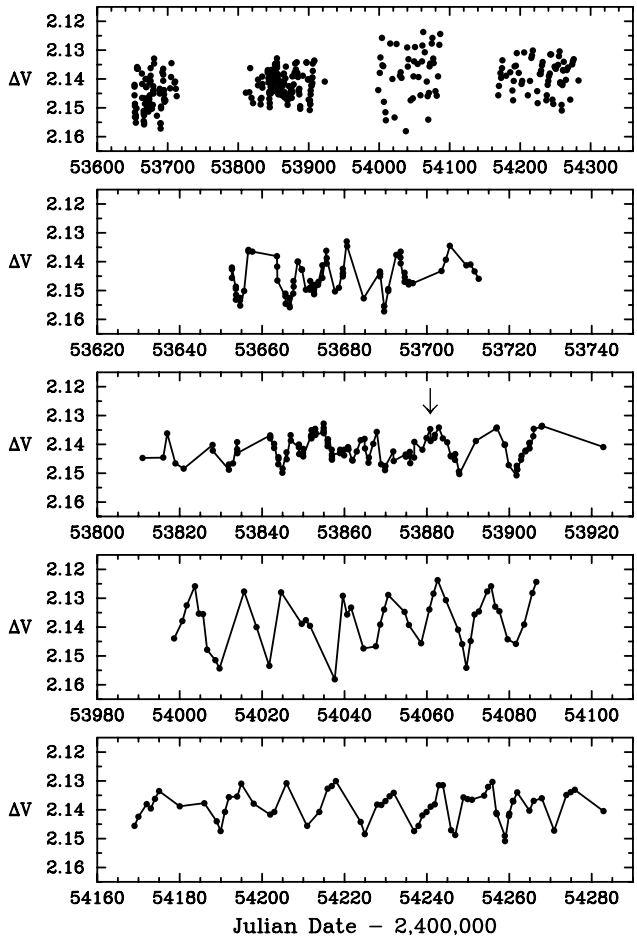

Figure 6.2: Figure from Henry & Winn (2008). They photometrically monitored HD189733 for 2 years. These plots show the magnitude difference between HD189733 and their comparison star, HD189410. The top panel is all the data, whereas the bottom four focus more closely on smaller portions of the observations.

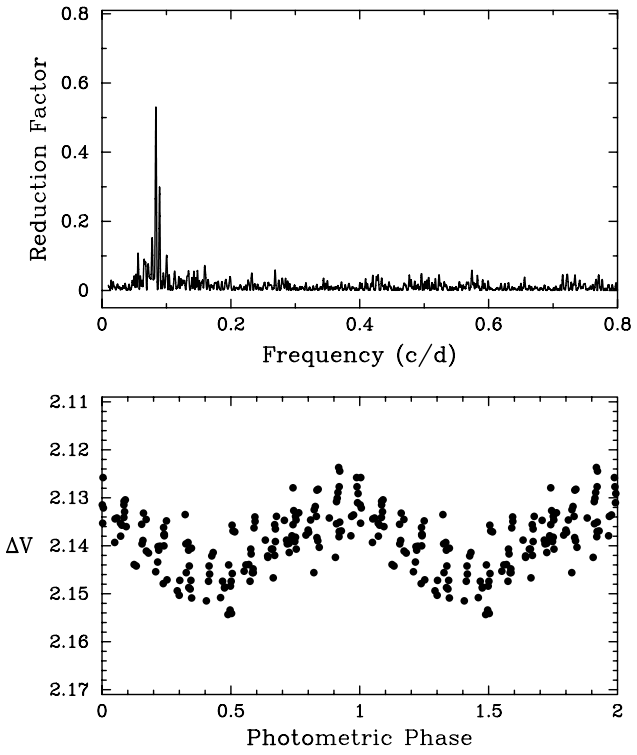

Figure 6.3: Figure from Henry & Winn (2008). They photometrically monitored HD189733 for 2 years. The variability of HD189733 is clearly shown here in a frequency power spectrum (top plot) of the data in 6.2 and the bottom is a phase-folded light curve using a period of 11.953 days.

Table 6.1: Final LDRs and linear fit parameters

transition 1 (nm)	transition 2 (nm)	intercept	slope	linear least squares residuals
554.6500	555.3688	−0.70376165	0.000389194	0.000162168
570.1104	570.3575	−1.6265429	0.000392078	0.000506895
570.1104	570.5473	−1.6120441	0.000431917	0.000320711
570.1104	570.5981	−1.1785547	0.000308887	0.000139829
570.1104	570.8089	−1.6461963	0.000459184	0.000879564
570.3575	570.5981	3.3065795	−0.000438695	0.000224084
570.5473	570.6997	−1.6828619	0.000473711	0.000530139
570.8089	570.8400	2.7167439	−0.000371122	0.000328444
570.8400	570.9378	−1.2646659	0.000367753	0.000586295
570.8400	570.9539	−1.3320775	0.000378494	0.00065165
575.4404	576.0842	2.5089003	−0.000361476	0.000893123
576.0345	576.0842	3.2373337	−0.000449928	0.000217316
576.0842	576.2415	−0.76642016	0.00031607	$7.88E-05$
592.2110	592.7786	7.6014335	−0.00124507	0.0007331
597.8543	598.4814	4.3831073	−0.000675594	0.00068775
597.8543	598.7066	5.2300573	−0.000822325	$8.35E-05$
610.3186	611.1066	3.0069103	−0.000316223	0.000754581
616.5361	617.7236	−1.3110832	0.000560265	0.000250532
621.9279	623.7319	5.886318	−0.000837754	0.000687511
622.0776	623.7319	2.1603572	−0.000327063	$2.62E-05$
622.6730	623.7319	2.8669116	−0.000419789	$3.00E-06$
622.9225	623.7319	4.861406	−0.000731017	$8.62E-05$
623.0726	623.7319	5.9847722	−0.000835582	0.000894876
623.2639	623.7319	4.9672125	−0.000689751	0.000408451
623.7319	624.0312	−1.7766535	0.000566664	0.000130981
623.7319	624.0645	−1.6199441	0.000464879	$5.08E-06$
628.5150	629.0969	7.7120605	−0.001292522	0.000156462
655.4224	656.9209	5.595728	−0.000939701	0.000156725
655.6062	656.9209	4.9990782	−0.000804644	0.000173389
655.6062	657.4225	2.5888801	−0.00033028	0.000839337
717.9993	718.9151	2.9030941	−0.000387802	0.000124404
724.4856	729.1447	2.8908101	−0.000344751	0.000443385
728.9175	729.3045	−0.7093027	0.00031161	0.000964686
734.4690	735.5935	2.5126818	−0.000330712	0.000730409
734.4690	736.1552	0.40861342	0.000338924	0.000206722
734.4690	738.9401	3.9211605	−0.000601219	0.000338902
734.4690	739.3613	5.5395801	−0.000890245	$3.18E-05$
734.4690	740.9346	4.3895375	−0.000684313	0.000291759
734.4690	741.4500	3.6122162	−0.000526033	0.000889166
735.3509	736.1552	−3.1807208	0.000792134	$8.24E-06$
735.3509	736.4097	−1.8112627	0.000445971	$8.61E-05$
735.5935	736.1552	−2.4684175	0.000970997	$7.55E-05$
735.5935	738.5236	2.8608012	−0.000302819	$7.24E-05$
735.5935	740.9346	2.7250557	−0.000319368	0.000130781
735.7726	738.5236	5.9512419	−0.000970842	$3.71E-05$
735.7726	739.3613	5.795651	−0.000953622	0.000615624
736.1552	738.9401	2.2709701	−0.000366867	$2.11E-05$
736.1552	739.3613	3.3005823	−0.000558119	$4.95E-05$
736.1552	740.1688	4.6672491	−0.00080173	0.000360748
736.1552	740.9346	2.5380059	−0.000415389	$2.76E-05$
736.1552	741.4500	2.0664799	−0.000318762	$1.05E-05$
736.4097	738.9401	4.5437164	−0.000745435	$7.86E-05$
736.4097	739.3613	6.376986	−0.001082612	$6.65E-06$
736.4097	740.1688	8.9209277	−0.001534311	0.000483734
736.4097	740.9346	5.0591735	−0.000839328	$7.57E-05$
736.4097	741.4500	4.2308201	−0.000670063	0.000262728
740.9083	740.9346	−1.4469623	0.000398484	0.000581881
740.9083	741.4500	−1.8134993	0.000473673	0.000274454
807.5146	808.5176	2.5723175	−0.000320769	0.000166404
819.8917	820.4935	−0.62255523	0.000316187	0.000115587
820.4935	820.7745	3.7125062	−0.000511351	0.000296563

Bibliography

Bakos, G. Á., et al. 2006, , 650, 1160

Biazzo, K., Catalano, S., Frasca, A., & Marilli, E. 2004, Memorie della Societa Astronomica Italiana Supplement, 5, 109

Bouchy, F., et al. 2005, , 444, L15

Caccin, B., & Penza, V. 2002, in ESA Special Publication, Vol. 477, Solspa 2001, Proceedings of the Second Solar Cycle and Space Weather Euroconference, ed. H. Sawaya-Lacoste, 205–208

Charbonneau, D., Irwin, J., Nutzman, P., & Falco, E. E. 2008, in Bulletin of the American Astronomical Society, Vol. 40, Bulletin of the American Astronomical Society, 403–+

exoplanet.eu. 2010, The Exoplanet Encyclopedia, `http://exoplanet.eu/index.php`

Fares, R., et al. 2010, ArXiv e-prints

Gray, D. F. 1976, The observation and analysis of stellar photospheres / David F. Gray (Wiley, New York :), xv, 471 p. ;

Gray, D. F. 1994, , 106, 1248

Gray, D. F., & Livingston, W. C. 1997, , 484, 511

Hall, J. C., Lockwood, G. W., & Skiff, B. A. 2007, , 133, 862

Henry, G. W., & Winn, J. N. 2008, , 135, 68

Knutson, H. A., Howard, A. W., & Isaacson, H. 2010, ArXiv e-prints

Koesterke, L., Allende Prieto, C., & Lambert, D. L. 2008, , 680, 764

Kovtyukh, V. V., Soubiran, C., Belik, S. I., & Gorlova, N. I. 2003, , 411, 559

Kurucz, R., & Bell, B. 1995, Atomic Line Data (R.L. Kurucz and B. Bell) Kurucz CD-ROM No. 23. Cambridge, Mass.: Smithsonian Astrophysical Observatory, 1995., 23

Luterbacher, J., Rickli, R., Tinguely, B., Beck, C., Pfister, C., & Wanner, H. 2004, Climatic Change

Observatory, E. S. 2010, eso.org, http://www.eso.org/public/

Ramsey, L. W., et al. 1998, in Society of Photo-Optical Instrumentation Engineers (SPIE) Conference Series, Vol. 3352, Society of Photo-Optical Instrumentation Engineers (SPIE) Conference Series, ed. L. M. Stepp, 34–42

Redfield, S., Endl, M., Cochran, W. D., & Koesterke, L. 2008, , 673, L87

Spatiales, C. N. D. 2010, CNES.fr, http://www.cnes.fr/web/CNES-en/7114-home-cnes.php

Tull, R. G. 1998, in Presented at the Society of Photo-Optical Instrumentation Engineers (SPIE) Conference, Vol. 3355, Society of Photo-Optical Instrumentation Engineers (SPIE) Conference Series, ed. S. D'Odorico, 387–398

van Belle, G. T., & von Braun, K. 2009, , 694, 1085

Wolszczan, A., & Frail, D. A. 1992, , 355, 145